



**Fermi National Accelerator Laboratory**

FERMILAB-Conf-89/26

## **Structure Functions and Parton Distributions\***

Wu-Ki Tung<sup>a,b,c</sup>, J. G. Morfin<sup>b</sup>, H. Schellman<sup>b</sup>, S. Kunori<sup>d</sup>, A. Caldwell<sup>e</sup>, F. Olness<sup>f</sup>

<sup>a</sup> Argonne National Laboratory, Argonne, Illinois 60439

<sup>b</sup> Fermi National Accelerator Laboratory, P.O. Box 500, Batavia, Illinois 60510

<sup>c</sup> Illinois Institute of Technology, Chicago, Illinois 60616

<sup>d</sup> University of Maryland, College Park, Maryland 20742

<sup>e</sup> Nevis Laboratories, Irvington-on-Hudson, New York 10533

<sup>f</sup> University of Oregon, Eugene, Oregon 97403

January 1989

\*To appear in the proceedings of the 1988 Summer Study on High Energy Physics in the 1990s, Snowmass, Colorado, June 27-July 15, 1988.



Operated by Universities Research Association, Inc., under contract with the United States Department of Energy

STRUCTURE FUNCTIONS AND PARTON DISTRIBUTIONS<sup>†</sup>Wu-Ki Tung<sup>a,b,c</sup>, J. G. Morfín<sup>b</sup>, H. Schellman<sup>b</sup>, S. Kunori<sup>d</sup>, A. Caldwell<sup>e</sup>, F. Olness<sup>f</sup><sup>a</sup>Argonne National Laboratory, Argonne, IL<sup>b</sup>Fermi National Accelerator Laboratory, Batavia, IL<sup>c</sup>Illinois Institute of Technology, Chicago, IL<sup>d</sup>University of Maryland, College Park, Md<sup>e</sup>Nevis Laboratories, Irvington-on Hudson, NY<sup>f</sup>University of Oregon, Eugene, OR

## Abstract

Parton distributions play an essential role in the QCD parton model in studies of all high energy processes in physics of the 1990's. The primary source of information on parton distributions is from structure functions measured in deep inelastic scattering experiments. In this report we: (i) review the current status of deep inelastic scattering experiments; (ii) closely examine common experimental practices and diverse analysis assumptions; (iii) evaluate the efficacy of currently used parton distribution parametrizations; (iv) report on our efforts to compile an extensive database on structure functions and to initiate a comprehensive study of the extraction of parton distributions from them; (v) present preliminary results and conclusions from this study; and (vi) discuss the important roles that current and near-future experiments (especially at the colliders) can play in the complete determination of parton distributions. Particular attention is placed on the gluon distribution and on the small- $x$  extrapolation problem. A concise summary of precise definitions of parton distributions and QCD parton model formulas are included in the introductory section to meet the increasing need of next-to-leading order applications of QCD.

<sup>†</sup> To appear in the Proceedings of the 1988 Summer Study on High Energy Physics in the 1990's, Snowmass, Colorado.

Other members participating in the Work-group on Structure Functions and Parton Distributions at Snowmass were: R. Blair, F. Borchering, J. Huston, G. Snow, and M. Zielinski.

- I. INTRODUCTION
- II. BASIC DEFINITIONS AND FORMALISM
  - A. STRUCTURE FUNCTIONS IN DEEP INELASTIC SCATTERING
  - B. PARTON DISTRIBUTIONS IN THE NAIVE PARTON MODEL
  - C. QCD PARTON MODEL FORMULAS
- III. REVIEW OF MEASUREMENTS OF STRUCTURE FUNCTIONS
  - A. REVIEW OF RECENT EXPERIMENTAL RESULTS
    - F2(x,Q): HEAVY TARGETS EXPERIMENTS
    - F2(x,Q): HYDROGEN TARGETS DATA
    - STATUS OF THE "EMC-EFFECT"
    - THE LONGITUDINAL STRUCTURE FUNCTION
    - Q-DEPENDENCE OF F2(x,Q) AND QCD
  - B. REVIEW OF ANALYSIS ASSUMPTIONS AND CORRECTIONS
    - GENERAL REMARKS
    - "STRANGE SEA" AND "ISOSCALAR" CORRECTIONS
    - "SLOW RESCALING" CORRECTION AND CHARM THRESHOLD
    - CONVENTIONS ON QUARK DISTRIBUTIONS
  - C. DATABASE ON STRUCTURE FUNCTIONS
- IV. REVIEW OF PARTON DISTRIBUTION FUNCTIONS
  - A. COMPARISON OF KNOWN PARTON DISTRIBUTIONS WITH DATA
  - B. EXPERIMENTAL ISSUES ON THE EXTRACTION OF PARTON DISTRIBUTIONS
  - C. NEXT-TO-LEADING ORDER EVOLUTION CALCULATIONS
- V. PROGRAM TO EXTRACT PARTON DISTRIBUTION FUNCTIONS
  - A. DESCRIPTION OF METHODS
  - B. PRELIMINARY RESULTS
  - C. TENTATIVE OBSERVATIONS AND CONCLUSIONS
- VI. ROLE OF CURRENT AND FUTURE EXPERIMENTS IN THE DETERMINATION OF PARTON DISTRIBUTIONS
  - A. FIXED TARGET LEPTON-HADRON SCATTERING
  - B. HERA
  - C. DRELL-YAN PROCESS
  - D. DIRECT-PHOTON PRODUCTION
- VII. SUMMARY
- ACKNOWLEDGEMENT
- REFERENCES

## I. INTRODUCTION

The QCD Parton Model provides a comprehensive framework for describing general high energy processes in current and planned accelerators and colliders. In this framework, a typical hadron-hadron collision process  $A + B \rightarrow C + X$ , where  $C$  represents a final state of physical interest, can be expressed in terms of more basic processes involving the elementary constituents (partons) of the fundamental theory as depicted in Fig.1.

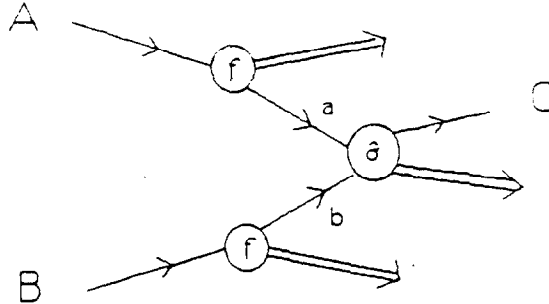


Fig.I-1: The QCD Parton Model

The physically measured cross-section for such a process is written in terms of a convolution of *Parton Distribution functions*  $f_A^a(x,Q)$  and *Hard cross-sections*  $\hat{\sigma}_{ab}$  which represent the fundamental physical processes initiated by the partons:

$$\sigma_{AB}(s \dots) = f_A^a(x_1 \dots) \otimes \hat{\sigma}_{ab}(\hat{s}, Q \dots) \otimes f_B^b(x_2 \dots) \quad (I-1)$$

Here  $s$  is the squared energy of the overall processes,  $\hat{s}$  is the corresponding quantity for the parton-parton subprocess,  $Q$  is an appropriate energy scale characteristic of the hard process (usually of the order of  $\sqrt{\hat{s}}$ ) and  $x_{1,2}$  are the fractional longitudinal momenta carried by the partons relative to the parent hadrons.

It is obvious from Fig.I-1 and Eq.(I-1) that the **parton distributions**  $f_A^a(x,Q)$  play a key role in any serious study of high energy process. *All quantitative relations between measured cross-sections and fundamental interactions of the theory require precise knowledge of these (universal) distribution functions.* The main source of information on the parton distributions come from **deep inelastic scattering Structure Functions**. The Group on Structure Functions and Parton Distributions at this Workshop was set up to review the current status of and to identify outstanding issues confronting the determination of the parton distributions for the study of physics of the 1990's, and to address these issues as much as possible.

The QCD Parton Model picture suggests that the kinematic variables  $(x,Q)$  are important in considering the physics potential of current and planned high energy facilities. In Fig.I-2, we show a Road Map of HEP for the 1990's which indicates the regions in the  $x$ - $Q$  plane of the physics reach of current and planned accelerators and colliders. The shaded region in the lower left corner represents that covered by current fixed-target deep inelastic scattering experiments where extensive information on structure functions are, in principle, available. It is clear from this map that extrapolations from this kinematic range to those of physical processes at the Tevatron and SSC are enormous in both  $Q$  and  $x$  variables. The theoretical tool for effecting the extrapolation to large  $Q$  (horizontal direction in Fig.I-2) is the **QCD evolution equation** which describes well the  $Q$ -dependence of structure functions within the range of available energies. On the other hand, much less is known about the extrapolation to small  $x$  (vertical direction in Fig.I-2). Available theoretical guides are qualitative and are

subject to change when further progress are made. Hence, it is particularly important to acquire *experimental* information on parton distribution functions in the small  $x$  region. To this end, *increasing reliance must be placed on studying hadron collider processes which are sensitive to parton distributions at small  $x$*  - at least before the e-p collider at HERA comes on line. (For practical purposes, "small  $x$ " means here  $x$  values below currently measured range, say less than 0.05, cf. Fig.I-2.)

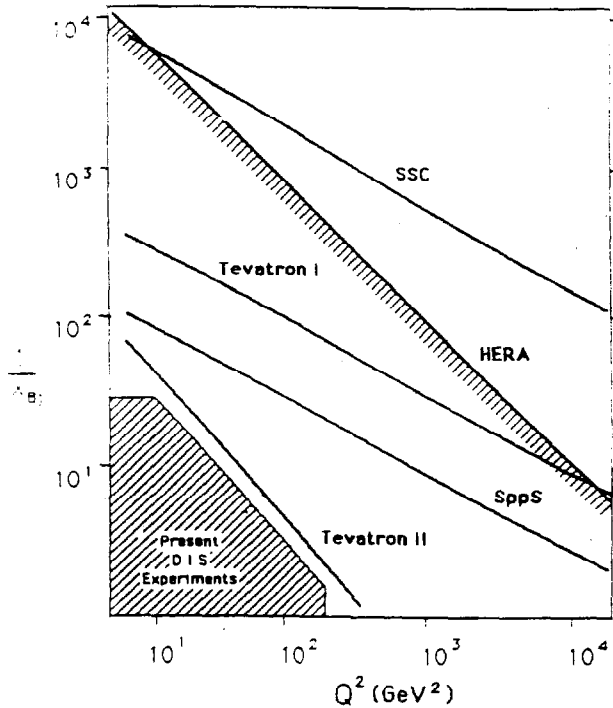


Fig.I-2: Road Map of High Energy Physics in the 1990's.

Recent developments in high energy jet physics, heavy-flavor production, lepton-pair production, direction-photon production, ... all point to the importance of including **higher order effects of the QCD parton model**, Eq.(I-1), if quantitative QCD analyses are to be made.<sup>1</sup> This requires not only the calculation of higher order hard cross-sections, as usually emphasized, but also the use of parton distribution functions derived with evolution kernels to the corresponding order in the QCD coupling parameter  $\alpha_s$ . For this reason, any serious study of parton distributions must spell out the precise definitions of these distributions, their relations to the measured structure functions, and their proper use in the general formula Eq.(I-1) which are *valid beyond the leading order* in QCD. With this in mind, the summary of the basic formalism given in Sec.II of this report serves as a guide to contemporary practitioners of the QCD Parton Model who are not necessarily experts of perturbative QCD.

## II. BASIC DEFINITIONS AND FORMALISM

For modern applications of the QCD Parton Model, it is essential to clearly distinguish the *universal Parton Distributions* from the *Structure Functions* measured in the *specific* Deep Inelastic Scattering experiments. The relation between the two is intimate, but by no means trivial beyond the leading order. Fig.II-1 illustrate this relationship:

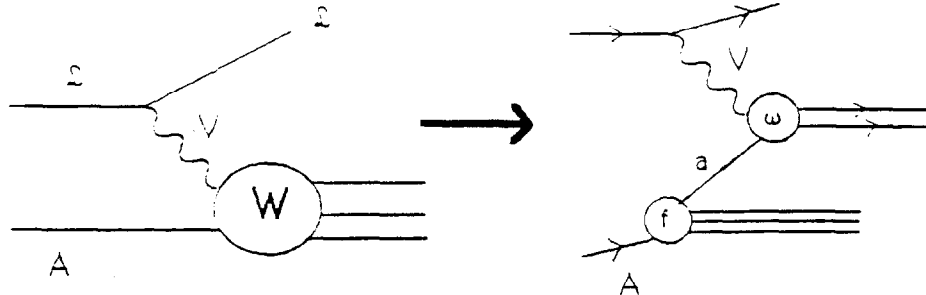


Fig.II-1: Deep Inelastic Scattering in the QCD Parton Model.

part (a) represents the *physically measurable structure functions* (to be denoted by  $W_A^i \cdot F_A^i$ ); part (b) represents the corresponding QCD Parton Model expression for these, in terms of a convolution of a *parton distribution function* ( $f_A^a$ ) (*soft wave function*) and a *Parton structure function* ( $\omega_a^i$ ) (*hard scattering of the vector boson probe V off the parton*).

In the naive parton model,  $\omega_a^i$  is represented by simple constant point-couplings of the partons, as shown in Fig.II-2a. In this approximation, the gluon does not contribute to the scattering in any direct way (all its couplings vanish); and the quarks do not couple to the longitudinal structure functions (the gauge coupling of the quarks are pure transverse). **Beyond the leading order**, the perturbatively calculable  $\omega_a^i$  become non-trivial (Fig.II-2b,c); the gluon will contribute directly (Fig.II-2c); and the longitudinal structure function is predicted to be non-vanishing. In fact, this leads to the most direct way to measure the gluon distribution, cf. Sec.II.C.

(a) Leading Order; (b) 1st Order Quark; (c) 1st Order Gluon.

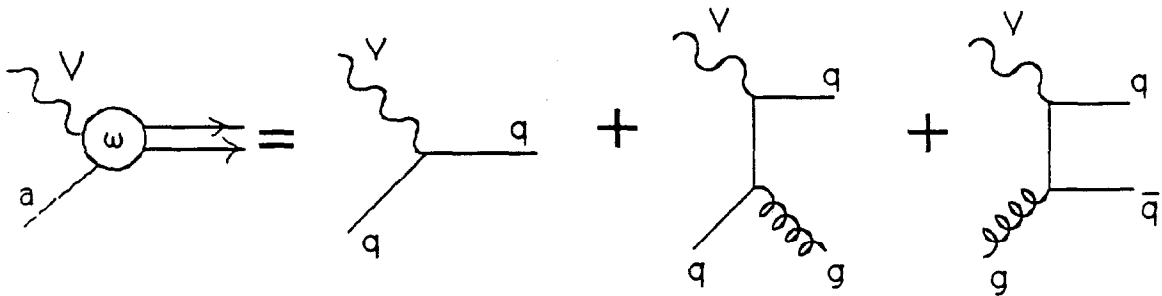


Fig.II-2 Perturbative series for the (hard) Parton Structure Function  $\omega$

Figs.II-1,2 should make it clear that the very definition of the parton distribution functions  $f_A^a$  depends on the approximation adopted for  $\omega_a^i$  — as the product must remain the same as the *physical* structure function. Beyond the leading order,  $\{\omega_a^i\}$  are necessarily renormalization-scheme dependent; hence, so are the parton distributions  $\{f_A^a\}$ . The following subsections are devoted to the definition of the physical structure functions, the leading order parton formulas and the next-to-leading order QCD parton formulas in turn.

## A. STRUCTURE FUNCTIONS IN DEEP INELASTIC SCATTERING

The generic deep inelastic scattering process depicted in Fig.II-1 are characterized by the well-known kinematic variables:

$$\begin{aligned} x &= \frac{Q^2}{2p \cdot q} & ; & & Q^2 &= q^2 = (\ell - \ell')^2 \\ \nu &= -q \cdot p / M = E - E' & ; & & W^2 &= -p'^2 = M^2 - Q^2 + 2M\nu \\ y &= q \cdot p / \ell \cdot p = (E - E') / E \end{aligned} \quad (II-1)$$

where  $E$  and  $E'$  are the laboratory energies of the leptons  $\ell$  and  $\ell'$  respectively, and the Lorentz metric is  $(-1,1,1,1)$ .

Taking into account the known lepton vertex in Fig.II-1, the cross-section for the overall process can be written in terms of **Structure Functions** ( $W_i$ ,  $i = 1, 2, 3$ ) as follows:

$$\begin{aligned} \frac{d\sigma^{\ell A}}{dx dy} &= N_V^{\ell} [2W_1^{VA}(x, Q) \sin^2(\theta/2) + W_2^{VA}(x, Q) \cos^2(\theta/2) \\ &\quad \pm W_3^{VA}(x, Q) \frac{E + E'}{M} \sin^2(\theta/2)] \end{aligned} \quad (II-2)$$

where  $(\ell, V, A)$  are labels for the (beam) lepton, the (exchanged) vector-boson and the (target) hadron respectively; the  $(\pm)$  signs are associated with  $(V = W^\pm)$ , i.e.  $\nu$ - and anti  $\nu$ - scattering; and  $\theta$  is the laboratory scattering angle. The process-dependent normalization constant  $N_V^{\ell}$  in (II-2) is given by:

$$N_V^{\ell \pm} = 8\pi\alpha^2 y E E' / q^4 \quad (II-3)$$

for electron and muon scattering, and

$$N_W^{\nu, \bar{\nu}} = \pi\alpha^2 y E E' / 2 \sin^4 \theta_w (q^2 + M_W^2)^2 \approx G_F^2 y E E' / \pi \quad (II-4)$$

for charged current neutrino- and antineutrino-scattering. When neutral-current weak interaction becomes important, the Z-exchange amplitude contributes by itself as well as through an interference term with the  $\gamma$ -exchange amplitude. The formulas for  $N_Z^{\nu}$  and  $N_Z^{\ell \pm}$  are not given here explicitly.

The structure functions  $W_i^{VA}$  are fundamental physical quantities for lepton-hadron scattering. They are proportional to the total cross-section of the relevant vector-boson - hadron scattering, hence (by the Optical Theorem) represent the imaginary part of the forward Compton scattering amplitude of  $V$  on  $A$ . The fundamental significance of the structure functions makes them the natural meeting ground between experiment and theory. In principle, the measurement of these structure functions in lepton-hadron scattering is independent of further theoretical assumptions, including the QCD parton model.

An alternate set of structure functions, commonly called  $F^i$  (or  $F^\lambda$ ), is motivated by the discovery of (approximate) scaling and the subsequent successes of the parton-model interpretation of deep inelastic scattering. The new structure functions are related to the  $W$ 's by the following relations.

$$\begin{aligned}
F^1 &= 2 W_1 & &= F^L - F^R \\
F^2 &= 2 \left( \frac{\nu^2}{q^2} + 1 \right) W_2 & &= F^L + F^R + 2F^{Long} \\
F^3 &= \frac{\sqrt{\nu^2 + q^2}}{M} W_3 & &= F^L - F^R
\end{aligned} \tag{II-5}$$

where the left-hand sides define  $F^i$  [ $i = 1,2,3$ ] in the *tensor* basis while the right-hand sides define  $F^\lambda$  [ $\lambda = L$  (*left-handed*),  $R$  (*right-handed*), and  $Long$  (*longitudinal*)] in the *helicity* basis. The boson and hadron indices as well as the arguments of the functions have been suppressed. It is seen that  $F^1$  represents the **transverse amplitude**,  $F^2$  the **sum of helicity amplitudes**, and  $F^3$  the **parity-violating amplitude**. For reference, the inverses of the above relations are:

$$F^{L,R} = \frac{F^1 \pm F^3}{2} \quad ; \quad F^{Long} = \frac{F^2 - F^1}{2} \tag{II-6}$$

Since neutrinos carry definite helicities, the cross-section formula Eq.(II-2) takes on a simple form in terms of the helicity structure functions in the deep inelastic scattering limit  $M^2/q^2 \ll 1$ :

$$\frac{d\sigma^{\nu A}}{dx dy} = \frac{G^2}{\pi} MEx \left[ \frac{F^L}{F^R} + 2(1-y) \frac{F^{Long}}{F^{Long}} + (1-y)^2 \frac{F^R}{F^L} \right] \tag{II-7a}$$

where the top line (with structure function boson sub-index +) applies to **neutrino-scattering**, and the bottom line (with structure function boson sub-index -) applies to **anti-neutrino scattering**. This is to be compared with the more often seen formula in terms of the tensor structure functions,

$$\frac{d\sigma^{\nu A}}{dx dy} = \frac{G^2}{\pi} MEx \left[ \frac{y^2}{2} F_{\pm}^1 + (1-y) F_{\pm}^2 \pm \left( y - \frac{y^2}{2} \right) F_{\pm}^3 \right] \tag{II-7b}$$

where  $\pm$  refers to neutrino and anti-neutrino scattering respectively.

It is to be noted that the above definitions of  $F^i$  with the tensor index ( $i$ ) are slightly different from the original definitions of the scaling structure functions found in the earlier literature and in experimental papers:

$$F^1 = 2 \cdot F_1^{org}; \quad F^2 = F_2^{org} / x; \quad F^3 = F_3^{org} \tag{II-8}$$

More and more recent theoretical papers use the new set defined by Eq.(II-5) because of the simple relations to the helicity amplitudes and to the parton model expressions for these quantities (cf. next section). It should be emphasized, however, that *all sets of structure functions are mere redefinitions of  $W_i$* ; and, as such, *they are just as fundamental and free from dynamical assumptions as the latter*. This fact is, unfortunately, not observed and respected in some experimental "measurements" where model-dependent (usually parton-model inspired) "corrections" were applied to the *structure functions* analyses. (Cf. Sec. III.B)

## B. PARTON DISTRIBUTIONS IN THE NAIVE PARTON MODEL

In general, quarks of different generations couple identically to the electro-weak gauge bosons and the gluon does not couple directly to them. To leading order in the QCD coupling, the parton structure functions  $\omega_a^i$  are just (squares) of these electro-weak coupling constants. Denoting by  $U(x)$  and  $D(x)$  the generic up-like (*u,c,t*) and down-like (*d,s,b*) quark probability distributions inside the target hadron ( $A$ ), respectively, the **electromagnetic structure functions** are given by:

$$F_{\gamma A}^{3, Long}(x) = 0 \tag{II-9}$$

$$F_{\gamma A}^{1,2}(x) = \frac{4}{9} \Sigma [U_A(x) + \bar{U}_A(x)] + \frac{1}{9} \Sigma [D_A(x) + \bar{D}_A(x)]$$

where the first sum (over the *generations*) includes all up quarks and anti-quarks, and the second sum includes all down and anti-down quarks. The **charged-current weak structure functions** are simplest when written in the *helicity basis* because of the basic left-handed weak coupling:

$$F_{+A}^L(x) = 2 \Sigma D_A(x) , \quad F_{+A}^R(x) = 2 \Sigma \bar{U}_A(x) \tag{II-10}$$

$$F_{-A}^L(x) = 2 \Sigma U_A(x) , \quad F_{-A}^R(x) = 2 \Sigma \bar{D}_A(x)$$

*Thus, these measured structure functions neatly sort out the up-quarks, down-quarks and the corresponding anti-quarks. We have, of course, again the result that the gluon distribution does not contribute to the structure functions; and that the longitudinal structure vanishes in this approximation:*

$$F_{VA}^{Long}(x) = 0 \quad \text{for all } V \tag{II-11}$$

For **isoscalar targets** (normalized to per nucleon cross-section and denoted by  $A=N$ ), we define

$$F_{VN}^i(x) = \frac{1}{2} [ F_{Vp}^i(x) + F_{Vn}^i(x) ] \tag{II-12}$$

Invoking **strong iso-spin invariance**, and singling out the first generation up and down quarks, we use the abbreviations:

$$f_p^{u,d}(x) = f_n^{d,u}(x) = u(x), d(x) \tag{II-13}$$

$$f_p^{s,c,b}(x) = f_n^{s,c,b}(x) = s(x), c(x), b(x)$$

Eq.(II-9) becomes

$$\begin{aligned}
F_{+N}^{1,2}(x) &= \frac{5}{18} (u+\bar{u}+d+\bar{d}) + \frac{1}{3} \Sigma' (U+\bar{U}) - \frac{1}{3} \Sigma' (D+\bar{D}) \\
&= \frac{5}{18} \Sigma (q + \bar{q}) + \frac{1}{6} \Sigma' (U+\bar{U} - D-\bar{D}) \\
&\approx \frac{5}{18} \Sigma (q + \bar{q}) + \frac{1}{3} \Sigma' (U - D)
\end{aligned} \tag{II-14}$$

Where  $\Sigma q$  indicates the sum over all quark flavors, and  $\Sigma'$  denotes the sum over all generations beyond the first. In the third line, one makes the additional assumption that at all values of  $x$ ,

$$U(x) = \bar{U}(x) \quad ; \quad D(x) = \bar{D}(x) \tag{II-15}$$

for all higher generations.

**For neutrino scattering on isoscalar targets, we obtain:**

$$\begin{aligned}
F_{+N}^L(x) &= d(x) + u(x) + 2s(x) + 2b(x) \\
F_{+N}^R(x) &= \bar{u}(x) + \bar{d}(x) + 2\bar{c}(x)
\end{aligned} \tag{II-16}$$

and for anti-neutrino scattering:

$$\begin{aligned}
F_{-N}^L(x) &= u(x) + d(x) + 2c(x) \\
F_{-N}^R(x) &= \bar{d}(x) + \bar{u}(x) + 2\bar{s}(x) + 2\bar{b}(x)
\end{aligned} \tag{II-17}$$

Note that the corresponding neutrino and anti-neutrino structure functions for iso-scalar targets differ only in the higher generation parton contents which are in general small at moderate values of  $x$ . *The left-handed and right-handed structure functions separately measure the quark distributions and the anti-quark distributions.*

**Now, consider the tensor structure functions for neutrino scattering:**

$$\begin{aligned}
F_{+N}^{1,2}(x) &= u + \bar{u} + d + \bar{d} + 2s + 2b + 2\bar{c} \approx \Sigma(q + \bar{q}) \\
F_{+N}^3(x) &= u - \bar{u} + d - \bar{d} + 2s + 2b - 2\bar{c} \\
&\approx \Sigma (q - \bar{q}) + 2(s+b-c) = \Sigma q_V + 2(s+b-c)
\end{aligned} \tag{II-18}$$

where  $\Sigma q(x)$  [ $\Sigma \bar{q}(x)$ ] represents the sum over all quark [anti-quark] flavors and  $q_V(x)$  is the *valence* quark distribution. For **anti-neutrino scattering**, we obtain:

$$\begin{aligned}
F_{-N}^{1,2}(x) &= u + \bar{u} + d + \bar{d} + 2\bar{s} + 2\bar{b} + 2c \approx \Sigma(q + \bar{q}) \\
F_{-N}^3(x) &= u - \bar{u} + d - \bar{d} - 2\bar{s} - 2\bar{b} + 2c \\
&\approx \Sigma q_V - 2(s + b - c)
\end{aligned} \tag{II-19}$$

Note that  $F_{\pm N}^3$  are dominated by their first term which is basically  $(u_v + d_v)$  where  $u_v$  and  $d_v$  denote the "valence" up and down quark distributions. The residue pieces in  $F_{\pm N}^3$  does not have definite flavor quantum numbers. Hence  $F_{\pm N}^3$  is, strictly speaking, not "non-singlet". That distinction applies to the combined neutrino and anti-neutrino structure function.

Neutrino and anti-neutrino structure functions are, *a priori*, different quantities. In the parton model they are closely related as shown above. It is common practice to form sums and differences of neutrino and anti-neutrino cross-sections within one experiment and extract the resulting structure functions. We begin with the case of **iso-scalar target** then consider the single hadron results. In the parton model, from the **sum of the cross-sections**, one obtains:

$$F_N^{2+}(x) = \frac{F_{+N}^2 + F_{-N}^2}{2} = \Sigma [\bar{q}(x) + q(x)] , \quad (II-20)$$

$$F_N^{3+}(x) = \frac{F_{+N}^3 - F_{-N}^3}{2} \approx 2 [s - c + b]$$

Thus the sum of cross-sections is dominated by the  $F^2$  ( $F^1$ ) structure function.

From the **difference of the two cross-sections**, one obtains:

$$F_N^{2-}(x) = \frac{F_{+N}^2 - F_{-N}^2}{2} = s - \bar{s} - c + \bar{c} + b - \bar{b} = 0 \quad (II-21)$$

$$F_N^{3-}(x) = \frac{F_{+N}^3 + F_{-N}^3}{2} \approx u_v + d_v$$

Hence the difference of cross-sections is dominated by the  $F^3$  structure function which measures the valence quark content of the (iso-scalar) hadron target.

For the general case of **non-isoscalar target** (e.g. the proton), we obtain, for the **sum of cross-sections**:

$$F_A^{2+}(x) = \Sigma [D(x) + \bar{D}(x) + U(x) + \bar{U}(x)] \quad (II-22)$$

$$F_A^{3+}(x) = \Sigma [D(x) + \bar{D}(x) - U(x) - \bar{U}(x)]$$

where the sum is over the flavor generations, and  $(U, D)$  denote the up and down quark distributions of any generation as before. For the **difference of cross-sections**, one gets:

$$F_A^{2-}(x) = \Sigma [D_v(x) - U_v(x)] \quad (II-23)$$

$$F_A^{3-}(x) = \Sigma [D_v(x) + U_v(x)]$$

where  $D_v = D - \bar{D}$ , and similarly for  $U_v(x)$ . We see that neither  $F_A^{3+}$  nor  $F_A^{1-}$  are necessarily small in general, being in each case related to the difference in the up and down quark distributions.

### C. QCD PARTON MODEL FORMULAS

To leading order in the QCD running coupling, all naive parton model formulas given above remain valid in form with the proviso that all parton distribution functions acquire a Q-dependence dictated by the first-order QCD evolution equation (the Altarelli-Parisi Equation): i.e.  $f_A^a(x) \longrightarrow f_A^a(x, Q)$ .

Going beyond the leading order, as is increasingly necessary in current QCD parton model analyses, one must use the perturbatively calculated parton structure functions  $\omega_a^i$  (cf. Fig.II-1) and the corresponding parton distribution functions  $f_A^a(x, Q)$  generated with evolution kernels of the next order in QCD coupling. Thus in the next-to-leading order, the formula corresponding to Fig.II-1 reads:

$$F_{VA}^i(x, Q) = \omega_{VA}^i(x/\xi, Q, \mu) \otimes f_A^a(\xi, \mu) \quad (II-24a)$$

where  $\otimes$  indicates a convolution integral over the parton fractional momentum variable  $\xi$  ( $x < \xi < 1$ ), i.e.

$$\omega \otimes f \equiv \int_x^1 \frac{d\xi}{\xi} \omega\left(\frac{x}{\xi}\right) f(\xi) \quad (II-24b)$$

The parton structure functions  $\omega_a^i$  in Eq.(II-24) are no longer simple constant coefficients, but are calculated in perturbative QCD to a given order in the effective coupling  $\alpha_s(\mu)$ :

$$\omega^i(z, Q, \mu) = \omega_0^i \delta(1-z) + \alpha_s(\mu) \omega_1^i(z, Q/\mu) \quad (II-25)$$

In Eq.(II-24),  $\mu$  is a renormalization scale parameter which necessarily arises in perturbation calculations beyond the tree approximation. In practice,  $\mu$  is usually chosen to be the physical variable Q, which then simplifies the expressions for  $\omega_a^i$  to a perturbation series in which the coefficient function in each order depends only on one variable (cf. Eq.(II-27) below).

The functions  $\omega_a^i$  have been calculated to one-loop order in the MS-bar subtraction scheme<sup>2</sup>. A well-known result is that the longitudinal structure function is no longer zero: both quarks and gluons give non-vanishing contributions to the sum over parton label (a) in Eq.(II-24) to this order. We have:

$$F_{VA}^{Long}(x, Q) = \frac{\alpha(Q)}{2\pi} [\omega_g\left(\frac{x}{\xi}\right) \otimes f_A^g(\xi, Q) + \omega_q\left(\frac{x}{\xi}\right) \otimes f_A^q(\xi, Q)] \quad (II-26)$$

where

$$\begin{aligned} \omega_g(z) &= 2 N_f \cdot T_R \cdot 4z(1-z) && \text{(gluon)} \\ \omega_q(z) &= C_F \cdot 2z && \text{(quarks)} \end{aligned} \quad (II-27)$$

Here  $C_F$  and  $T_R$  are the usual QCD group factors and  $N_f$  is the number of quark flavors. Since the quark distributions can, to a large extent, be determined from the leading-order analysis of  $F^2$  and  $F^3$ , the first-order QCD relation between  $F^{long}$  and the parton distributions, Eq.(II-25), can therefore be used to precisely define, and to determine the gluon distribution. This is extremely important because knowledge on the gluon distribution is crucial in understanding the quantitative features of most hadronic processes at high energies,

and that direct handles on the gluon distribution are very hard to come by. We shall come back to the above equations in a later section on HERA.

In addition to their dependence on the renormalization scale  $\mu$  as indicated above, *the perturbative expressions for  $\omega_a^i$  are also renormalization scheme dependent.* Although they are usually calculated in the **MS-bar scheme**, other schemes have been advocated in various applications as being more practical. Since *the physical structure functions* (the left-hand sides of Fig.II-1 and Eq.(II-24)) *must be independent of renormalization schemes*, the scheme-dependence of  $\omega$  necessarily implies that *the parton distributions  $f_A^a(x,Q)$  are also renormalization-scheme-dependent constructs beyond the leading order in QCD.* This fact is becoming increasingly relevant because most recent "QCD analyses" by both theorists and experimental groups use the next-to-leading order formalism. Although some of these analyses explicitly specify the choice of renormalization scheme, others implicitly use a scheme which may be different from the commonly accepted ones. (Cf. Sec.III.B) Hence, it is desirable to describe here explicitly the definitions of these schemes.

The **MS-bar scheme** does not require further elaboration; one simply apply Eqs.(II-24,25) with the published MS-bar 1-loop parton structure functions  $\omega$  (Wilson coefficients).<sup>2</sup> In this scheme, all structure functions  $F^i(x,Q)$  acquire 1st order corrections of the form given in Eq.(II-24). The alternative schemes (to be called **DIS schemes** from now on) take advantage of the freedom to shift finite terms between the two factors in Eq.(II-24), and *choose to define parton distributions such that one of the deep inelastic scattering structure functions retains its simple leading order relationship to these distributions.* Because  $F^2(x,Q)$  is the best experimentally measured structure function, it is common in theoretical papers which elect to use this approach to choose this structure function for simplification. Explicitly, we have, for neutrino scattering off iso-scalar targets, as an example,

$$\begin{aligned} \text{and} \quad F^2(x,Q) &= \Sigma (q^{(2)} + \bar{q}^{(2)}) \\ F^1(x,Q) &= F^2(x,Q) - 2 F^{Long}(x,Q) \end{aligned} \quad (II-28)$$

to 1-loop order, where  $F^{Long}(x,Q)$  is given by Eq.(II-26). The superscript in parentheses makes explicit the scheme dependence of this definition of the parton distributions and identifies  $F^{(2)}$  as the defining structure function.

There is an obvious alternative choice which picks the pure transverse structure function  $F^1(x,Q)$  (Cf. Eq.(II-5) to retain its simple relationship to parton distributions. In that case, Eq.(II-28) becomes:

$$\begin{aligned} \text{and} \quad F^1(x,Q) &= \Sigma (q^{(1)} + \bar{q}^{(1)}) \\ F^2(x,Q) &= F^1(x,Q) + 2 F^{Long}(x,Q) \end{aligned} \quad (II-29)$$

We shall call these two schemes **DIS-2** and **DIS-1** respectively. Note that *these differing schemes result in different definitions of parton distributions* (distinguished by the superscript in parentheses); *the physical structure functions must remain the same.*

In both of the above schemes,  $F^3(x,Q)$  acquires a non-trivial 1-loop correction (similar to the expression for  $F^{Long}(x,Q)$ ) which we shall not reproduce here. Since the helicity structure functions  $F^{R,L}(x,Q)$  are linear combinations of  $F^{1,3}(x,Q)$  (cf. Eq.(II-6)), they both have non-trivial corrections in these schemes. It is however possible to define two more distinct schemes (say, **DIS-R** and **DIS-L**) such that either  $F^R(x,Q)$  or  $F^L(x,Q)$  is given simply as sums of anti-quark or quark distributions respectively. This is an important point

in the experimental determination of anti-quark distributions in neutrino scattering because the "leading" term and the 1st order "correction" can be numerically comparable, as we shall see in Sec.III.B.

It is worth noting also that, *in contrast to the situation with the MS-bar scheme, Eqs.(II-28.29) and variations thereof cannot be used to define "DIS schemes" beyond the 1-loop order.* Both  $F^1(x,Q)$  and  $F^2(x,Q)$  must acquire higher order corrections beyond 1st order. In Sec.III.B we shall review the conventions used by the major experimental groups, and in a later section on parton distributions (Sec.IV.C) we shall discuss the numerical differences between the MS-bar-scheme distributions and their counterparts in the DIS-2 scheme.

Because of the inter-dependence of  $f_A^a(x,Q)$  and the parton cross-section  $\hat{\sigma}$ , Eq.(I-1), and structure functions  $\omega_a^i$ , Eq.(II-24), any meaningful application of the QCD Parton Model to high energy physical processes **beyond the leading order** must use parton distribution functions *defined in the same scheme and calculated to the corresponding order in perturbation theory* as the latter. In particular, to match *next-to-leading* hard cross-sections in Eqs.(I-1) and (II-24), one must use Q-dependent parton distributions derived with *two-loop evolution kernels*. Otherwise, the formulas will not be consistent. New results on next-to-leading order parton distributions will be reviewed in Sec.IV.C.

### III. REVIEW OF MEASUREMENTS OF STRUCTURE FUNCTIONS

Major strides have been made in the last few years in obtaining very high statistics data on deep inelastic scattering structure functions from electron-, muon- and neutrino-experiments on a variety of targets. In spite of this impressive progress, however, some noticeable differences remain which have caused a great deal of attention and concern. This section briefly reviews the status of the experimental measurements of structure functions and highlights any significant disagreements. In section V, we will comment on the implication of these differences on the extraction of parton distributions.

#### A. REVIEW OF RECENT EXPERIMENTAL RESULTS

<b>MUON EXPERIMENTS</b>			
	BCDMS	BFP	EMC
Target	C and H <sub>2</sub>	Fe	H <sub>2</sub> D <sub>2</sub> Fe
Energy	100 - 280	93, 215	120 - 280
x-range	.06 - .80	.08 - .65	.03 - .65
Q <sup>2</sup> -range	25 - 280	5 - 220	3 - 200
* events	C: 680K	690K	Fe: 1080K
R(x, Q <sup>2</sup> )	Expt.	0.0	0.0

Table III-1: Major recent Muon Experiments.

<b>NEUTRINO EXPERIMENTS</b>				
	BEBC	CCFRR	CDHSW	CHARM
Target	Ne H	Fe	Fe	Marble
Energy	10 - 200	30 - 250	30 - 300	10 - 200
x-range	.025 - .80	.02 - .65	.02 - .65	.02 - .55
Q <sup>2</sup> -range	2 - 70	1 - 200	0.2 - 200	0.2 - 100
R(x, Q <sup>2</sup> )	R(QCD)	R(QCD)	R(QCD)	0.1
* Events	25K	170K	940K	160K
SU(3) symmetry	$\bar{s} = 0.25 (\bar{u} + \bar{d})$ $c = \bar{c} = 0$		$\bar{s} = 0.2 (\bar{u} + \bar{d})$ $c = \bar{c} = 0$	
Charm	slow rescale: $m = 1.5$		No correction	

Table III-2: Major recent charged-current Neutrino Experiments.

Tables III-1 and III-2 summarize some key features of the more recent high statistics muon and (charged-current) neutrino experiments, including their kinematic ranges and important corrections applied. An understanding of the latter is extremely important if results from these experiments are to be combined in any quantitative model analyses, as there exist considerable differences in definitions and practices among the experiments. The second part of this section addresses some of these practices.

It is obvious from the above tables that these experiments are very extensive in their coverage. The cross-section measurements furnish, in principle, detailed information on the structure functions  $F_{\gamma,\nu}^{2,3}(x,Q)$  and  $F_{\gamma,\nu}^{long}(x,Q)$  (cf. Sec.II.A). The best determined structure functions are  $F_{\gamma,\nu}^2$  which correspond to combinations of the sum of quark and anti-quark distributions in the parton model. Unfortunately, because  $F_{\nu}^3$  and  $F_{\gamma,\nu}^{long}$  are determined by differences of cross-sections (Eqs.(II-5,6), hence the errors are more substantial. Similar limitations have so far discouraged efforts to separate the helicity structure functions which contain much more specific information on the parton content of the hadron. (Cf. Eq.(II-10))

Before comparing these measurements, it should be noted that *differences are expected* due to systematic effects, which are experiment dependent, and due to the different kinematical regimes covered by experiments. The impact of this last point is shown in Fig.III-1. Note that at the same value of  $x$  the average value of  $Q^2$  can differ by as much as an order of magnitude between various experiments. Care must be taken to remove this "natural" difference before comparing measurements.

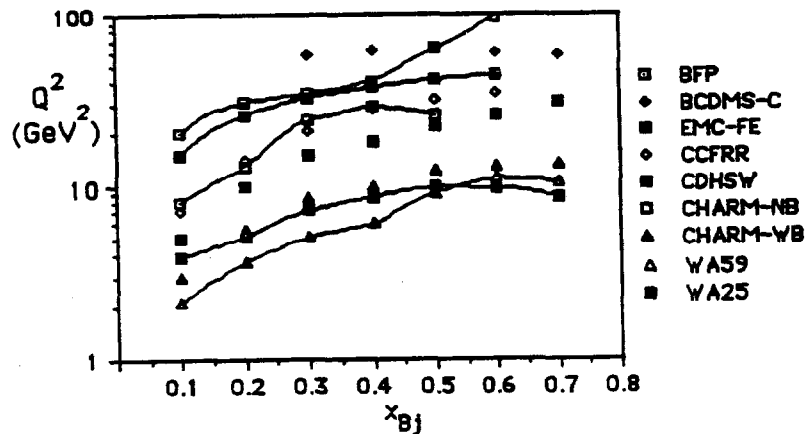


Fig.III-1: The dependence of  $\langle Q^2 \rangle$  on  $x$  for the various experiments.

### $F^2(x,Q)$ : Heavy Targets Experiments

Because of the relatively small neutrino cross-section, most of the high statistics experiments have used heavy targets (i.e. iron) detectors. Muon experiments, on the other hand, can get sufficient statistics even with hydrogen or deuterium targets. We will discuss the relation between heavy and light target results — the "EMC-effect" — shortly, but first we examine the ratio of the structure function  $F^2(x,Q)$  as measured by the heavy target experiments. The black points on Fig.III-2 represent this ratio between the two high statistics muon experiments, EMC on iron<sup>3</sup> and BCDMS on carbon<sup>4</sup>.

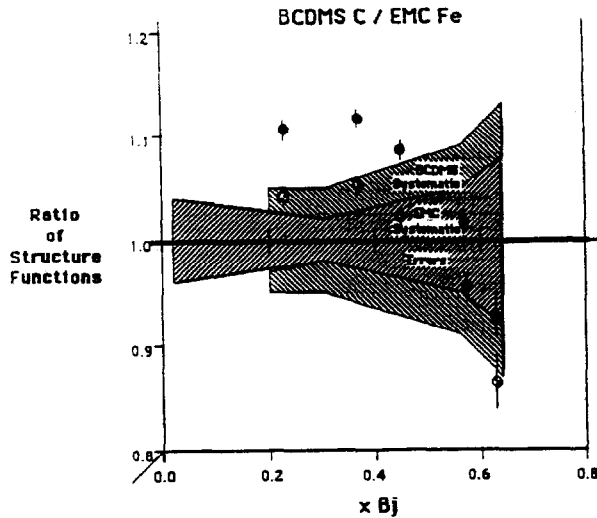


Fig.III-2: The Ratio of  $F^2(x,Q)$  measured by BCDMS and EMC on heavy targets (see text).

The error bars on the individual points are statistical and the systematic error from each experiment is shown in the cross-hatched area. The black/white points on the plot show the effect of a 5% change in relative normalization between the two experiments. There are no low  $x$  points since the high minimum  $Q$  of the BCDMS carbon experiment translates to a minimum  $x$  of about 0.2. The first thing one notices is the  $x$ -dependent trend of the ratio. However, the sum of systematic errors also depends on  $x$ . As illustrated by the black/white points, a 5% normalization change brings the "disagreement" within the band of systematic error. We note that, even though both experiments were done in the same beam at CERN, each measured the flux independently so a relative offset is possible.

The following set of figures show the ratio of  $F^2(x,Q)$  measured by the other heavy target experiments BFP<sup>5</sup>, CCFRR<sup>6</sup>, and CDHSW<sup>7</sup>, always with respect to EMC.

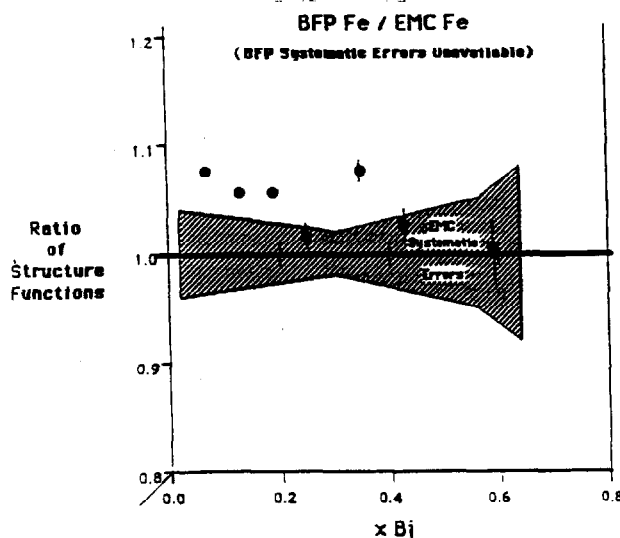


Fig.III-3: Ratio of BFP and EMC structure functions.

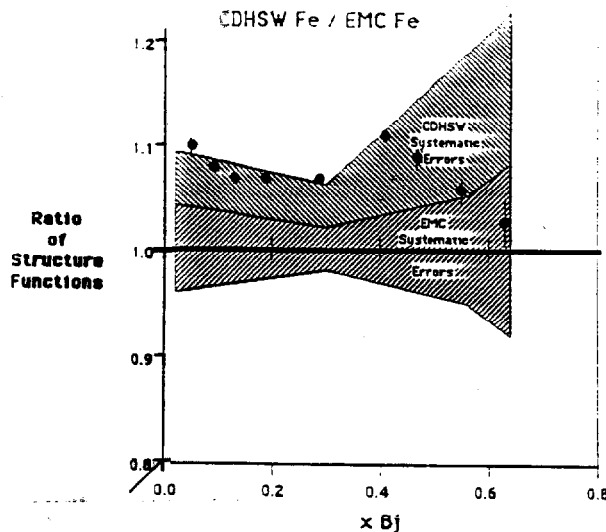


Fig.III-4: Ratio of  $F^2(x,Q)$  CDHSW and EMC experiments.

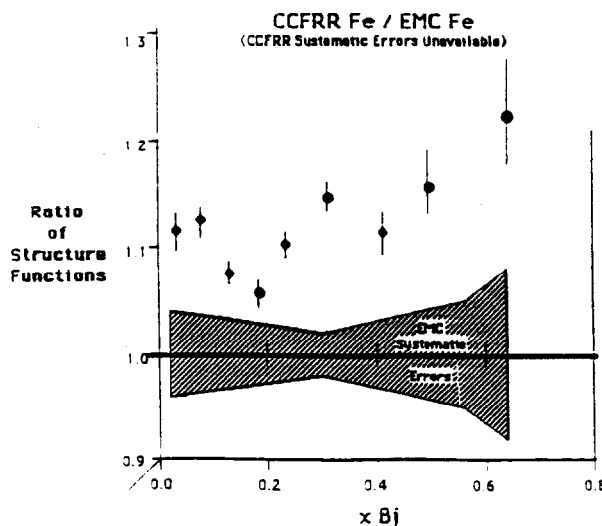


Fig.III-5: Ratio of  $F^2(x,Q)$  CCFRR and EMC experiments.

When comparing neutrino to muon results, a well-known parton-model motivated constant  $5/18$  has been applied, hence neglecting the small- $x$  contribution from the strange and charm sea quarks to this factor (cf. Eqs.(II-14,18)). The systematic errors for the CCFRR and BFP points are not shown (they should be comparable to the EMC error shown in the plots). In all cases, a shift in scale of a few percent statistically eliminates any discrepancy.

This report will concentrate on charged-current structure functions where detailed measurements exist. We shall only mention here that there is one new result from the Fermilab-MIT-MSU neutrino collaboration (E594)<sup>8</sup> which measures the neutral-current structure functions and compares the resulting quark distributions with those found in charged-current experiments. The comparison bears out the consistency of the quark parton model.

## $F^2(x,Q)$ : Hydrogen Targets Data

Fig.III-6 shows the ratio of  $F^2(x,Q)$  as measured by the two muon experiments BCDMS<sup>9</sup> and EMC<sup>10</sup> using a hydrogen target in each case. There is a pronounced  $x$ -dependent trend in this ratio similar to the heavy target case shown earlier.

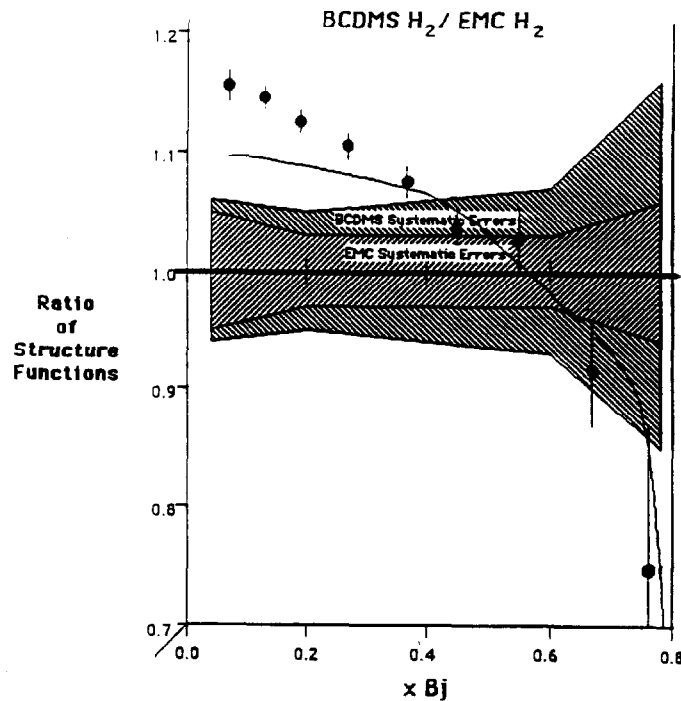


Fig.III-6: The Ratio of  $F^2(x,Q)$  measured by BCDMS and EMC on hydrogen target (see text).

However, in this case, no shift in relative normalization can eliminate the differences; there is clearly a statistically significant difference between these two high statistics experiments. The curve drawn represents an attempt by R. Mount<sup>11</sup> to simulate the ratio by assuming a 10% relative normalization mismatch and an assumed error in the BCDMS muon energy measurement of  $0.5 \text{ GeV} + 0.6\% E_{\mu}$ . We see that even these extreme assumptions cannot force an agreement between the two sets of data.

### Status of the "EMC-Effect"

New data on non-trivial  $x$ -dependence in the ratio of  $F^2(x,Q)$  measured on heavy targets and that on light target (deuterium)<sup>12</sup> come from SLAC E140<sup>13</sup> and EMC<sup>14</sup>. These new results are plotted along with earlier ones in Fig.III-7. They confirm the general feature that the ratio is below 1 at very low  $x$ , rises above 1 toward a maximum around  $x \approx 0.15$ , and then steadily decreases until  $x \approx 0.7$  before rising again.

There have been many attempts to explain this effect. It is generally agreed that shadowing effect is important below  $x = 0.1$ ; and nuclear effects are responsible for the observed effect above 0.1. For detailed model studies and earlier references, we refer the reader to two recent papers on this subject.<sup>15,16</sup> From a phenomenological point of view, it is obvious that this experimental ratio must be taken into account in any serious QCD parton model analysis which makes use of heavy target data on structure functions.

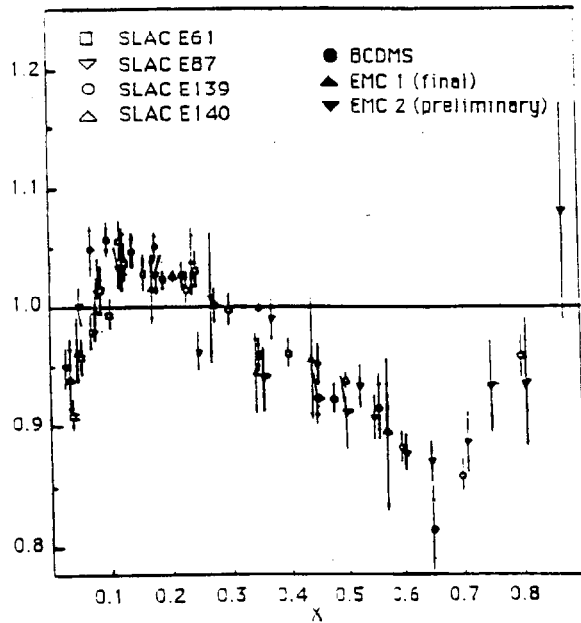


Fig.III-7: Combined data on the ratio  $F^2(\text{nucleus})/F^2(D_2)$

In contrast to the generally agreed  $x$ -dependence, experimental evidence on possible  $Q$ -dependence is unclear. F. Taylor<sup>17</sup> recently tried to fit current data to the ansatz:

$$\frac{d (F_2^{Fe} / F_2^D)}{d (\ln Q^2)} = (.077 \pm .023 \pm .047) - (.25 \pm .09 \pm .14) x \quad (\text{III-1})$$

( $\pm$  statistical  $\pm$  systematic). The data and fit are shown in Fig.III-8.

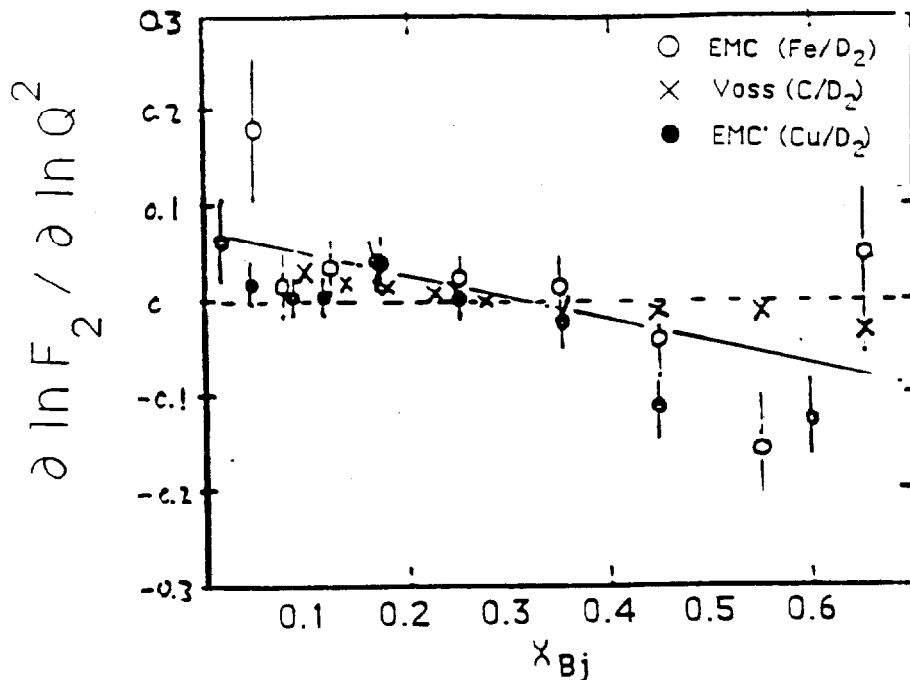


Fig.III-8: Possible  $Q$ -dependence of the EMC ratio.

## The Longitudinal Structure Function

There have been numerous experiments attempting to measure the ratio  $R(x,Q) = F_2^{long}(x,Q)/F_2(x,Q)$ . An indication of the accuracy of the current measurements is shown in Fig.III-9.

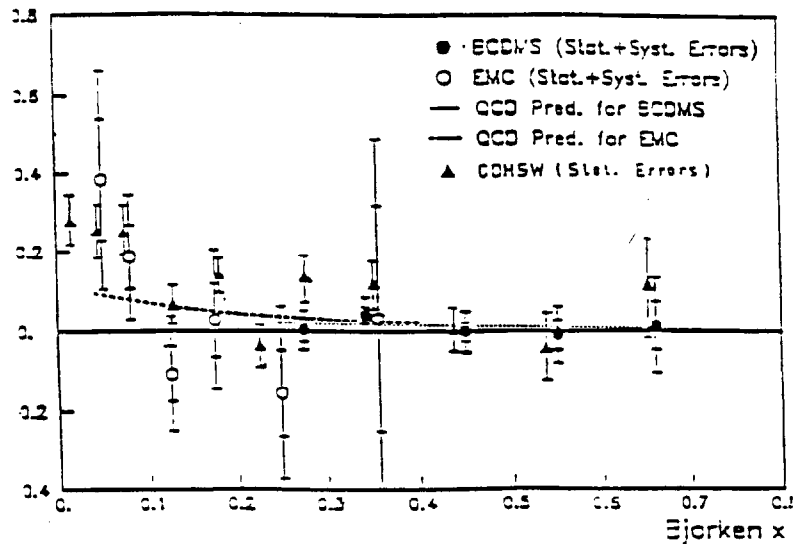


Fig.III-9:  $R(x)$  as measured by CDHSW, EMC and BCDMS.

A new impressive effort by the SLAC E140 experiment obtained very good data in the low- $Q$  region. The measured ratio is much larger than that given by the QCD formula Eq.(II-26), as is known for a long time. Any understanding of these data must go beyond the traditional twist-2 perturbative QCD, as mass threshold and other "higher-twist" effects still play an important role. Unfortunately, there is no real theory on these effects. An *ad hoc* prescription for including the so-called target mass effect seems to fit the data quite well, as seen in Fig.III-10.<sup>18</sup>

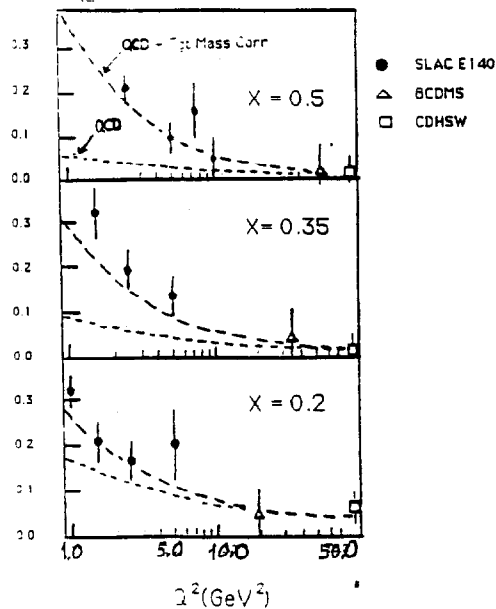


Fig.III-10:  $Q$ -dependence of the Ratio  $R$ .

### Q-dependence of $F^2(x,Q)$ and QCD

The Q-dependence of the structure functions is usually characterized by their logarithmic derivative, e.g.  $d(\ln F^2(x,Q))/d(\ln Q^2)$ . It is well known that this slope function has a definite x-dependence which is often taken as a good test of QCD predictions on the Q-evolution of structure functions. In the last two years, a lot of attention has been drawn to the fact that this measured slope function from the EMC and CDHSW experiments do not agree well with QCD.<sup>19</sup> Fig.III-11 shows the comparison between the experimental values and "the best fit" to next-to-leading order QCD. It has been pointed out<sup>20</sup> that as the minimum Q of the data is raised, the quality and the stability of the fit improve dramatically.

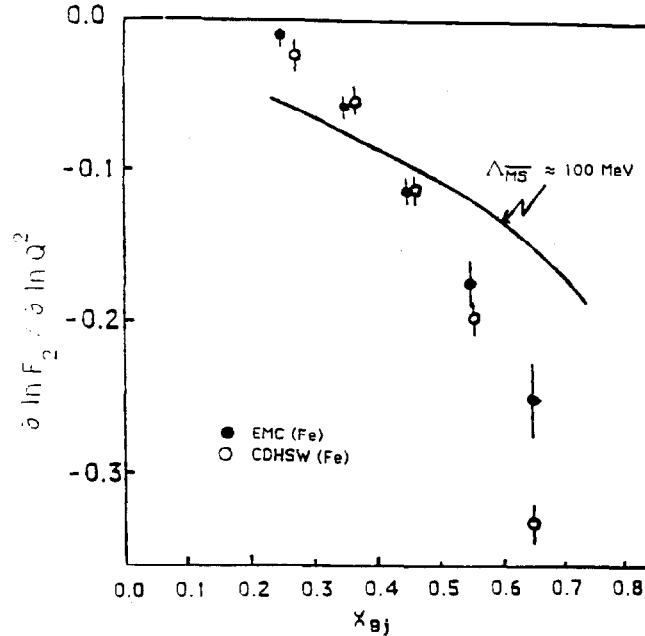


Fig.III-11: Slope of Q-dependence: EMC & CDHSW vs. QCD.

In contrast to the above, the recent BCDMS carbon and hydrogen data yield slope functions perfectly consistent with QCD. The result is reproduced in Fig.III-12.

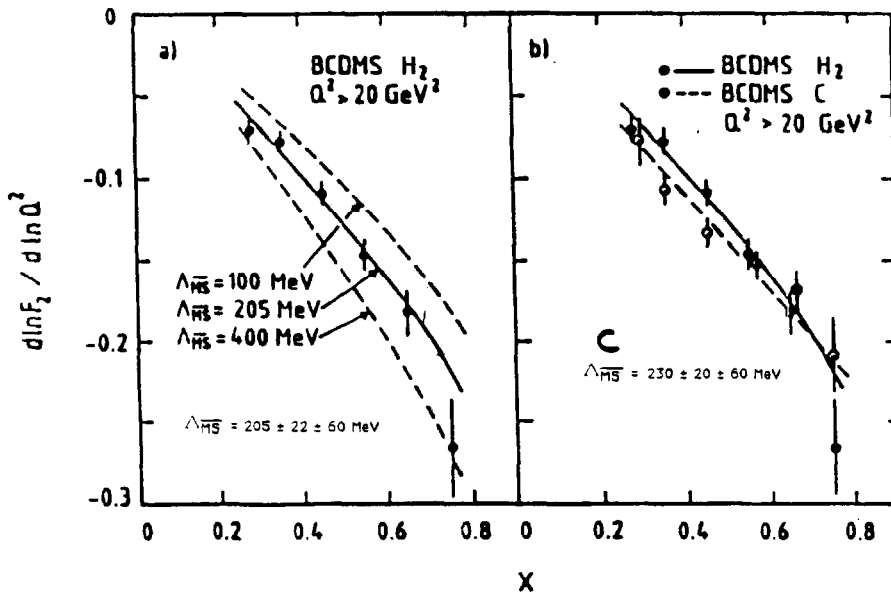


Fig.III-12: Slope of Q-dependence: BCDMS vs. QCD.

The BCDMS group obtained good fits to QCD formulas (cf. Sec.II.B,C) with QCD coupling parameter  $\Lambda_{\text{QCD}}$  slightly over 200 MeV in the MS-bar scheme. Consistent values were obtained by fitting to data above  $x = 0.25$  using the non-singlet formula without the gluon and by fitting to the data over the entire  $x$  range including gluon effects.<sup>21</sup>

A possible way to reconcile the QCD slope predictions with the EMC and CDHSW data was suggested by F. Taylor: if one applies a  $Q$ -dependent heavy-target correction to the structure function, as mentioned in the section on the "EMC-effect", one can write,

$$\frac{\partial \ln F_2^{Fe}}{\partial \ln Q^2} = \frac{\partial \ln F_2^D}{\partial \ln Q^2} + \frac{\partial \ln R^{Fe/D}}{\partial \ln Q^2} \quad (\text{III-2})$$

Then the QCD fit to the EMC data is improved as shown in Fig.III-13. A similar improvement was found for the BFP fit.

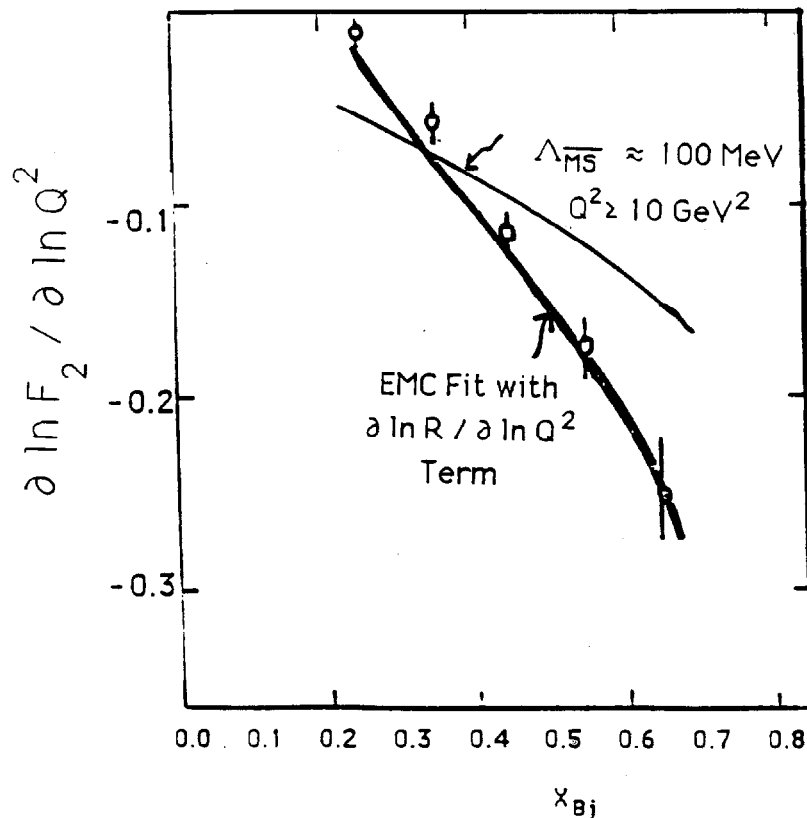


Fig.III-13: QCD fits to the EMC Fe data with and without the  $Q$ -dependent heavy-target correction.

## B. REVIEW OF ANALYSIS ASSUMPTIONS AND CORRECTIONS

### General Remarks

As seen in the previous section, the statistical power of the world's data on deep inelastic scattering structure functions has increased enormously. Because of the diminishing statistical error, correlations, systematic errors, and small differences in analysis assumptions become the dominant factors in the comparison of experimental data.

The major sources of systematic error — beam flux, energy calibration and detector acceptance — are strongly correlated from  $(x, Q)$  bin to bin. Thus, strictly speaking, they cannot be simply added to the statistical errors as they are not independent. For most of the recent experiments (but not all), information on separate systematic errors, including the sign of the effects, are available. In neutrino experiments, the statistical errors on  $F^2(x, Q)$  and  $F^3(x, Q)$  are also correlated for each bin. Thus, the correlation coefficient is needed in a comprehensive global fit.

Each major experiment adopts a unique procedure to extract structure functions from measured cross-sections. In order to make meaningful use of the published results, close attention must be given to the analysis assumptions used in the various experiments as they are often not the same. In this section, we briefly review procedures and practices used by the major experiments which are most relevant to QCD parton model analyses, and critically examine some of them.

When individual experiments perform a "QCD analysis" of their measured structure functions, most of the experimental considerations mentioned above are, of course, taken into account. There is, however, the question of definitions which are not standardized. In particular, the precise meaning of " $\Lambda_{\text{QCD}}$ " and the definition of anti-quark distributions vary in the published papers when "2nd order QCD analyses" are involved (Cf. Sec.II.C). The experimental considerations become a real problem when data sets are combined to make global fits by third parties. Since a lot of the relevant information are not even available in published form, the common practice is, more often than not, to ignore them. This clearly can lead to problematic results with uncertain errors.

In principle, measurement of the deep inelastic scattering structure functions should be independent of any theoretical model assumptions, as emphasized in Sec.II.A. For instance, six independent structure functions could be separately measured from the  $y$ -distributions of neutrino and anti-neutrino scattering for fixed  $(x, Q)$ . In practice, because experiments have limited coverage and/or efficiency over the kinematic range, only two combinations of cross-sections (roughly speaking, the sum and differences of neutrino and anti-neutrino cross-sections) are normally used to extract the published structure functions  $F^2(x, Q)$  and  $F^3(x, Q)$  respectively. When doing this, parton-model based expressions for the other four structure functions are introduced as corrections. Since the structure functions are, in turn, used as the main source of information to determine parton distributions, this is at best an iterative procedure. For serious QCD analyses, it clearly raises the concern of being a circular process. An open question is: *which of these corrections are really necessary, and which are used because of "accepted practice" and of over-reliance on the parton model.*

## "Strange Sea" and "Isoscalar" Corrections

Specifically, the structure functions usually quoted in the literature correspond to, in the notation of Sec.II,  $F^{2+}=(F^2_+ + F^2_-)/2$  (Eqs.(II-20,22)) and  $F^{3-}=(F^3_+ - F^3_-)/2$  (Eqs.(II-21,23)). In order to extract these functions, the following procedure is usually adopted to treat the other combinations: (i)  $F^{Long}(x,Q)$  is estimated from independent experimental measurements (y-distribution) or from the QCD formula Eq.(II-26) using assumed  $F^2(x,Q)$  and  $G(x,Q)$  functions, or is set equal to some small constant; (ii) since  $F^{2-}$  is given by  $(d_v - u_v)$  in the parton model (Eqs.(II-21,23)) it is expected to vanish for iso-scalar targets. Hence for targets close to being iso-scalars, it is assumed to be small; and an estimated **iso-scalar correction** is used to account for its contribution to the cross-section; (iii) the function  $F^{3+}$  is related in the parton model to the difference between all down-like quarks and up-like quark distributions (Eq.(II-22)), hence is proportional to the difference between the strange and charm quark distributions for iso-scalar targets (Eq.(II-20)). Since this is again expected to be small, an estimated **strange-sea correction** is applied to the cross-section to remove its effect. Using these (model-dependent) assumptions, no information on the y-distribution is needed for the determination of the two main structure functions.

## "Slow Rescaling" Correction and Charm Threshold

The QCD parton model provides an unambiguous formalism only when  $Q$  is much larger than the mass scales of the relevant process. For charged-current neutrino scattering, the production of charmed particles introduces a mass-scale at the charm threshold, which leads to complications in the parton-model interpretation of the structure functions for  $Q$  values of a few GeV. It is important to emphasize that *this complication only arises in the parton picture, it is not intrinsic to the determination of structure functions as basic physical quantities* as underlined in Sec.II.A. Hence there is no compelling physical reason to make a correction for this effect when structure function are measured.

In neutrino scattering, charm production is 5-10% of the total cross-section. There are two ways to confront the charm threshold problem when one makes a QCD parton analyses of charged-current structure functions. Either one imposes a  $Q^2$ -cut sufficiently above the charm quark mass so that the charm quark behaves as a light quark, threshold effects (this is one form of "higher-twist" effect) can be neglected, and the QCD formalism applies unambiguously; or one can apply a charm-mass correction to the structure functions with the purpose of preserving the parton language even at low  $Q$  but at the risk of working with highly model-dependent parton distributions. The choice between these two alternatives is clearly subjective. The analyses to be presented in later parts of this report use  $Q^2$ -cuts in the selection of data, and closely monitor the dependence of the physical output on the choice of the cut.

CCFRR and BEBC<sup>22</sup> choose to "correct" their measured structure functions for the charm-mass effect. The most often used method is termed the **slow rescaling correction**. As this directly affects the comparison of published experimental results, we give a brief summary of the commonly used procedure to do this.<sup>23</sup> First, in order to ensure that the final-state (charm) quark in the parton structure function  $\omega_a^1$  (Fig.II-2a) be an "on-shell" parton, the momentum fraction of the initial parton ( $s$  or  $d$ ) becomes

$$\xi = x (1 + M_c^2/Q^2)$$

rather than the familiar Bjorken  $x$ . Parton distribution functions are written as functions of  $(\xi, Q)$  instead of  $(x, Q)$ . Secondly, to take into account the existence of a minimum energy for charm production, a threshold multiplicative factor of  $\Theta(1 - xyM_c^2/\xi Q^2)$  is introduced for those terms leading to charm production in the parton formulas for the structure functions. For example, the normal parton expression  $x s(x, Q)$  is replaced by

$$\cos^2 \theta_c \xi s(\xi, Q) \Theta\left(1 - \frac{xyM_c^2}{\xi Q^2}\right) + \sin^2 \theta_c x s(x, Q)$$

and similarly for the other flavors.

CCFRR and BEBC *correct* for charm-mass effects to arrive at structure functions " $F^2(\xi, Q)$ " and " $F^3(\xi, Q)$ " which, according to this procedure, are interpreted as the equivalent zero-charm-mass structure functions (which have the usual simple relations to the "parton distributions"  $f(\xi, Q)$  in this scheme). CDHSW, on the other hand, defines their structure functions in the standard model-independent way as formulated in Sec.II. Vallage<sup>30</sup> made an explicit comparison of these two different definitions of structure functions. His result is shown in Fig.III-14. The differences at low  $Q^2$  are obviously significant!

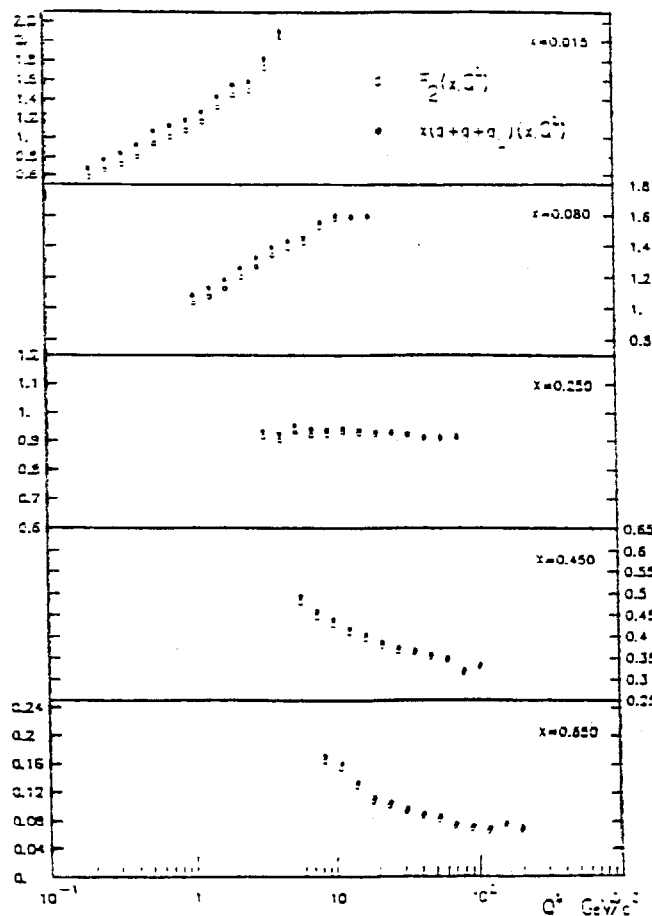


Fig.III-14: Comparison of  $F^2(x, Q)$  and "slow-rescaling corrected"  $F^2(x, Q)$ .

Because there is no reliable quantitative theory for threshold effects (these are fundamentally non-perturbative), and because the significance of structure function transcends the parton model, it is clearly desirable to retain the model-independent definition. Without standardization, published data on "structure functions" from different experiments actually correspond to different quantities, hence cannot be used in a meaningful way by anyone except the original experimental group. Thus, the potential usefulness of the laboriously obtained experimental data can be severely limited by model-dependent corrections. We strongly recommend that all experiments publish the standard structure functions without the slow-rescaling correction.

*It is, needless to say, interesting and tempting to explore parton-model interpretations of the measured structure functions even to low  $Q$  values, but that exercise should be conceptually distinguished from structure function measurements. In this case, the charm threshold problem must be faced and some form of slow-rescaling correct has to be applied. Since this correction usually requires information on the beam spectrum and the weighting of events which go beyond the structure functions, it would be extremely helpful if the published experimental papers also include tables of the measured cross-sections. This will maximize the usefulness of the experimental results, clarify the parton model analysis by the experimental groups (and others using their results), and minimize the possibility of unnecessary confusion and controversy.*

### Conventions on Quark Distributions

Most major experiments perform some form of QCD analysis and determination of parton distributions with their data. There are many subtleties and potential sources of confusion both due to intrinsic physics considerations and due to the different procedures and definitions used by different groups.

One problem concerns the treatment of the longitudinal structure function. Most experiments either measure  $F^{Long}(x,Q)$  independently or use an estimate for it in their determination of the other structure functions. Thus, experimentally  $F^1(x,Q)$  and  $F^2(x,Q)$  are not equal: they differ by  $2 \cdot F^{Long}(x,Q)$ . In leading order QCD, on the other hand,  $F^{Long}$  vanishes and  $F^2$  and  $F^1$  are supposed to be equal. Thus *parton model analyses at this level has an inherent ambiguity in their determination of the parton distributions*, depending on which of these experimental structure functions is used in the calculation. This results in real differences in that the muon experiments (BCDMS, BFP, and EMC) and CHARM<sup>24</sup> identify the sum of quark and anti-quark distributions with  $F^2(x,Q)$  whereas CCFR and CDHSW identify this combination of parton distributions with  $F^1(x,Q)$ .

To avoid this ambiguity, one must go beyond the leading order in QCD. Then the relationship between the structure functions and the parton distributions are no longer simple, and careful attention must be given to the explicit definition and the consistent use of a renormalization scheme, as explained in Sec.II.C. Since this level of the QCD parton model has not yet become a part of the folklore, confusion frequently arise when experimental results and naive parton model parlance are freely used in some detailed QCD analyses.

A specific case in point is the determination of the "anti-quark distribution" in neutrino experiments. The measured physical quantity is the coefficient of the  $(1-y)^2$  term in the neutrino cross-section which, according to Eq.(II-7), is just the right-handed helicity structure function  $F^R(x,Q)$ . Experimentally, this quantity is relatively small compared to

$F^2(x,Q)$ ; it is *numerically comparable* to  $F^{Long}(x,Q)$  at low values of  $Q$ . However, in the QCD parton model formalism,  $F^R(x,Q)$  is formally of *leading order*, in contrast to  $F^{Long}(x,Q)$ . To this order, it is simply proportional to the sum of anti-quark distributions as given by Eqs.(II-10,16). The ambiguity described in the previous paragraph now comes into full play when one tries to determine the quark distributions by combining  $F^R(x,Q)$  with  $F^2(x,Q)$  or  $F^1(x,Q)$  -- *the ambiguous term* (i.e.  $2 \cdot F^{Long}(x,Q)$ ) *is numerically comparable* to  $F^R(x,Q)$ , supposedly the "anti-quark-distribution" one is trying to subtract.

As mentioned earlier, the obvious way out of this dilemma is to go to the next order in QCD where this ambiguity is absent. In that case, however, one must accept the fact that the direct relationship between  $F^R(x,Q)$  and the anti-quark distributions is drastically modified in general -- the 1st order "correction term" to the naive parton formula which links the two may be comparable to the "leading term" because the latter starts numerically small (cf. Eq.(II-28,29) and the two paragraphs following these equations). One can, as explained in Sec.II.C, choose a convention (i.e. the DIS-R scheme) in which the anti-quark distributions are still simply related to  $F^R(x,Q)$ . In doing so, however, all other structure functions acquire non-trivial corrections.

For next-to-leading order QCD analyses, all muon experimental groups use the DIS-2 scheme definition of parton distributions (in the terminology of Sec.II.C) for which  $F^2(x,Q)$  retains its simple interpretation as the sum of quark and anti-quark distributions, but all other structure functions acquire non-trivial corrections to 1-loop order. The CHARM collaboration also explicitly use this scheme in their QCD analysis. The other neutrino experiments have not yet presented full next-to-leading order QCD analyses. To the extent that they usually identify  $F^1(x,Q)$  with the sum of quark and anti-quark distributions, they are effectively using the DIS-1 scheme defined in Sec.II.C. As pointed out in the previous paragraph, *the relationship between the anti-quark distribution and the measured  $F^R(x,Q)$  is not simple in either of these schemes*. Users of the quark and anti-quark distributions extracted by the experimental groups should be very careful in ensuring that the convention used in the experimental analysis is consistent with the applications.

We close this section on review of experimental practices with one more observation. In view of the observed target-dependence of the structure functions (i.e. the EMC-effect, cf. Sec.III.A), the CHARM collaboration makes a *correction* to their measured structure functions based on the measured A-dependence from the muon experiments.<sup>12</sup> None of the other experiments adopt this practice. This appears to be wise, for the same reasons as those described in the section on charm mass corrections. Such corrections are best applied at the time of specific applications.

### C. DATABASE ON STRUCTURE FUNCTIONS

One of the main purposes of this study group is to compile a consistent database of measured structure functions which can be used in further quantitative QCD analyses. The work on extracting parton distributions, to be reported in Sec.V, is an example of such a analysis. Our goal is to produce computer readable files with structure functions and error estimates for all recent experiments in a common format for easy access and to have available other relevant information on analysis methods for easy comparison.

We would like to include in the data base: the structure function values, the statistical errors, any statistical correlation with other values (e.g.  $F^2(x,Q)$  and  $F^3(x,Q)$ ), and separate

error estimates for each of the major sources of systematic error for each data point. Each file will be accompanied by a list of the analysis assumptions used (such as those discussed in previous subsections) in the extraction of the structure functions.

As noted above, in structure function measurements, the major sources of systematic error are often calibrations, acceptance, or normalizations which are highly correlated from point to point. With separated systematic errors, one can better assess the effect of experimental uncertainties (say, a 1% shift in beamline energy calibration) on the determination of physical quantities (such as  $\Lambda_{\text{QCD}}$ ).

We currently have essentially complete files for some experiments (BCDMS, CDHSW, and EMC). Information on the other experiments are not complete because they are not published and are not yet accessible to us. We strongly urge experimental groups to publish their data and to include as much complete information on systematic effects and cross-sections as possible.

#### IV. REVIEW OF PARTON DISTRIBUTION FUNCTIONS

Deep inelastic scattering Structure Functions are the primary source of our knowledge on the Parton Distribution Functions inside a hadron. The extraction of the latter from the structure functions is based on the QCD formula (II-24) (cf. Fig.II-1). The extensively used parton distribution functions of Gluck-Hoffman-Reya,<sup>25</sup> Duke-Owens,<sup>26</sup> and Eichten-Hinchliffe-Lane-Quigg (EHLQ)<sup>27</sup> were deduced from experimental data available up to the early 1980's; they were based on the leading order approximation to the QCD formula plus specific assumptions about the form of the initial distributions at a given  $Q_0$ . Recently, two new sets of distributions, based on next-to-leading order QCD calculations and on comparison to newer experimental data, have been made available to the high energy physics community.<sup>28,29</sup>

In order to assess the reliability of these distributions as input to quantitative QCD Parton Model applications and as tools for extrapolation from the measured fixed target energy range (the shaded area in the  $x$ - $Q$  plot of Fig.I-2) to the kinematic region of current and future collider processes (cf. Fig.I-2), we examine: (i) how well do the available parton parametrizations reproduce the measured deep inelastic scattering structure functions (as reviewed in Sec.III); (ii) what are the important factors which must be considered in a meaningful fitting program to extract the parton distributions from DIS experiments, and whether they have been taken into account in existing fits; and (iii) whether the existing next-to-leading order calculations are consistent and reliable, especially in the small- $x$  region where the evolution kernel has a singular behavior. These points have not been systematically studied in the published literature so far. All of them have significant bearing on the central question of concern: how much does current data constrain the behavior of the parton distributions in the extrapolation to small- $x$  and large  $Q$ ? The small- $x$  question is especially important because of the dearth of firm theoretical knowledge on this issue, and because all interesting high energy cross-sections depend sensitively to this extrapolation.

##### A. COMPARISON OF KNOWN PARTON DISTRIBUTIONS WITH DATA

We have systematically compared recent data on structure functions with parton model calculations based on the standard parton distribution functions mentioned above. Space limitation only permits the presentation of typical results from representative data sets and parton parametrizations. In Fig.IV-1 we show the high statistics BCDMS- $H_2$ , CDHSW-Fe,<sup>30</sup> and EMC- $H_2$  structure functions  $F_2(x,Q)$  plotted against  $Q$  for various different  $x$ -bins. For each experiment, data are divided into two plots: those with  $x < 0.3$  and with  $x > 0.3$ . To avoid overlapping data points and for clarity of display, the small  $x$  plots correspond to  $F_2^2(x,Q)/x$  in log scale, whereas the large  $x$  plots correspond to  $xF_2^2(x,Q)$  in linear scale. The 4 curves shown on each plot are obtained from the parton model formulas, Eqs.(II-14) and (II-18), using the parametrizations of EHLQ-1, Duke-Owens-1, MRS-E, and DFLM-FXAVR respectively. We see significant departure of some of these curves from the experimental data, for small- $x$  in general, and for moderate  $x$  as well in the case of the BCDMS data. Not shown here are the corresponding results for  $F_3(x,Q)$ . The agreement between data and existing parametrizations there is much better, although the error bars on the experimental data points are considerably bigger.

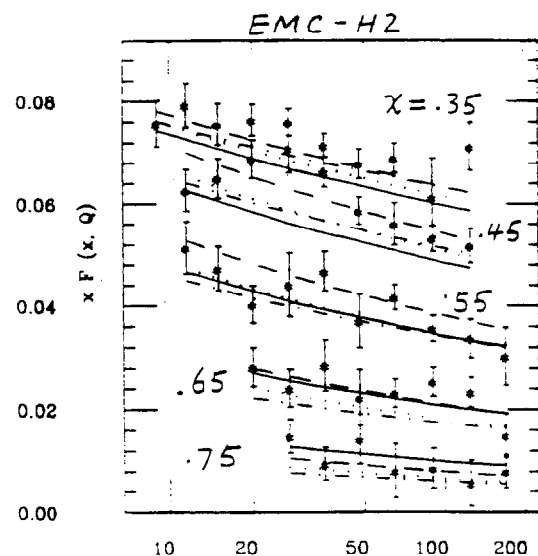
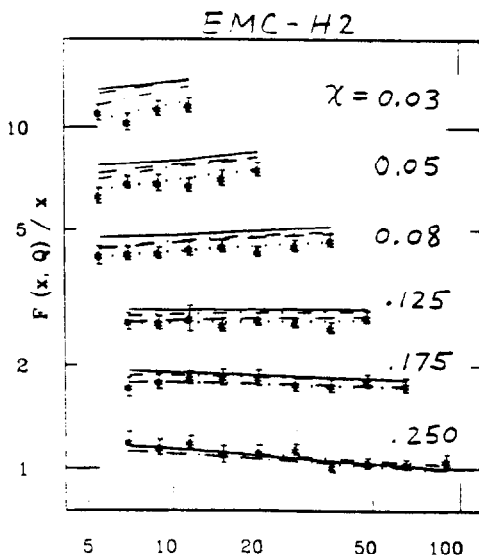
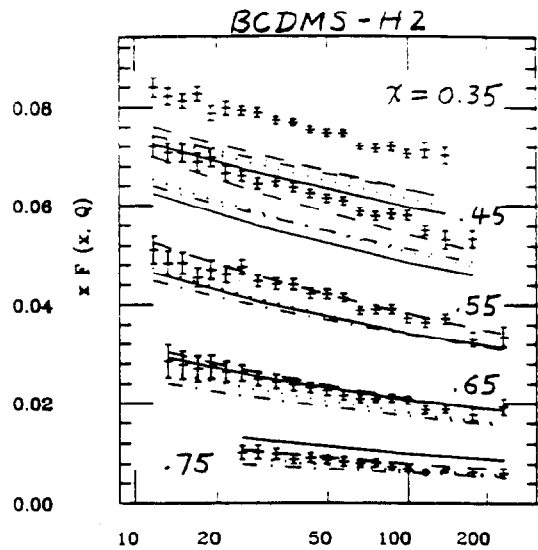
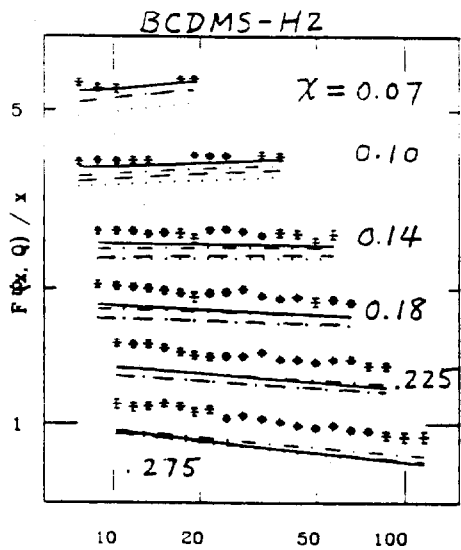
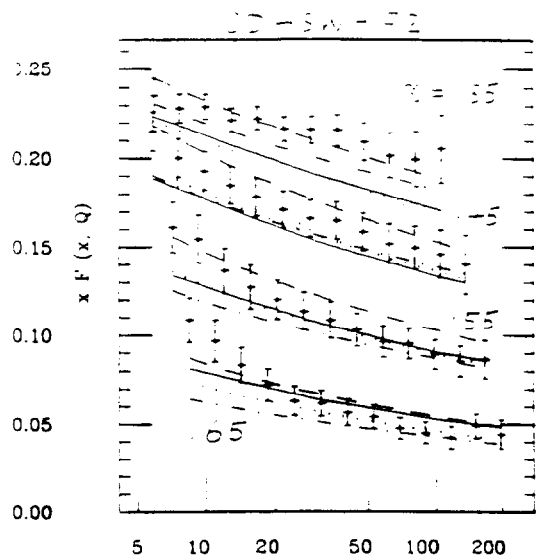
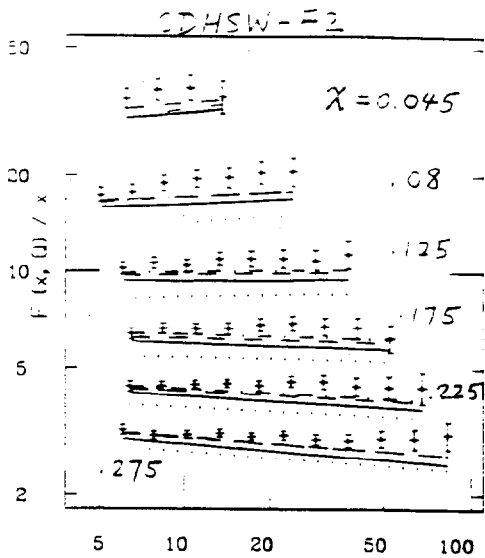


Fig.IV-1: Comparison of  $F^2(x, Q)$  measured in CDHSW, BCDMS ( $H_2$ ) and EMC ( $H_2$ ) experiments with calculated values from representative parton distribution sets: Duke-Owens-1 (dashed curve), ELHQ-1 (dotted), DFLM-FXAVR (solid), and MRS-E (dash-dotted).

Since the curves shown above are obtained the same way most "predictions" of the QCD-parton model are calculated, these graphs give a reasonable over-all picture of the quality of existing parton distributions *in the currently accessible energy range*. (Extrapolation is not involved here!) It is not possible to discuss here in detail the sources of the observed disagreement. The main factors are: (i) most standard parametrizations were obtained by fitting only one, or few, set(s) of data; (ii) in some kinematic regions, the new data sets are different from those of the early 1980's on which the first-generation parametrizations were obtained; and (iii) most authors allow a relative normalization scale between data points from different experimental sets in the fitting procedure, which cannot be included in the above comparison or any practical application. A notable example of how the discrepancy arises is given by the widely used EHLQ distributions which were derived primarily from the 1983 CDHS data. The latter were obtained using values for the total cross-section which later measurements have determined to be around 10% too low.<sup>31</sup> Thus the EHLQ distributions lead to structure functions conspicuously away from the new data points as shown in Fig.IV-1.

The above comparison makes the need to determine more up-to-date parton distributions obvious. Also apparent from the plots is the fallacy of the often used statement to the effect that *parton model predictions based on different existing parton parametrizations should bracket the true answer and give an estimate of the theoretical uncertainties*.

## B. EXPERIMENTAL ISSUES ON THE EXTRACTION OF PARTON DISTRIBUTIONS

In order to extract reliable parton distributions (inside the proton) from the measured structure functions in a quantitative analysis, it is, in principle, necessary to take into account: (i) systematic errors of the experimental data used, (ii) corrections due to differences of structure functions on heavy targets from those on light targets (the "EMC effect"), (iii) significant correlations of structure functions measured in the same experiment, and (iv) the variety of "corrections" applied by the experimental groups in extraction of the structure functions (which are often different from experiment to experiment). (Cf. Sec.III) In practice, a review of the original papers reveal that previous efforts to extract parton distributions, with few exceptions, mostly ignore these considerations. A necessary condition for incorporating all relevant factors is to have a comprehensive data base which include these details. Our effort to compile such a database has been described in Sec.III.C.

## C. NEXT-TO-LEADING ORDER EVOLUTION CALCULATIONS

Nominally, the inclusion of the second-order evolution kernel in the calculation of the scale-dependent parton distribution functions yields order  $\alpha_s/\pi$  (about 10%) corrections to the leading order results. However, this is not necessarily true over all kinematic regions. Just as in the case of hard scattering cross-sections,<sup>1</sup> there are circumstances under which the higher order kernel can be significant, or even dominant, compared to the leading one. This consideration is especially relevant for small-x because, in many respects, the region of small x is exceptional.<sup>32</sup> (For instance, the evolution kernel is singular at  $x = 0$ . Certain elements of the second-order kernel, in fact, is more singular than the leading-order one; hence they can become quite important.) It is extremely important to determine how the rapid growth of the parton distribution functions with the energy scale in the small-x region (on which projected large cross-sections for physical processes in future colliders are based) is affected by the inclusion of second order effects.

The implications of the second order kernel on the predicted behavior of parton distributions, especially in the small- $x$  region has been recently studied in a systematic manner.<sup>33</sup> This investigation confirmed and quantified the significance of the 2nd order effect. Fig.IV-2 illustrates the difference between 1st and 2nd order evolution of the parton distributions. Shown are the momentum distribution of the u-quark and the gluon at  $Q = 15$  GeV, obtained from 1st and 2nd order calculations which start with the same set of distributions at  $Q_0 = 3$  GeV and which use the same effective coupling strength. We see significant differences in the small- $x$  region but only small variations above  $x = 0.05$ . The 2nd-order u-quark distribution is 35% higher than the 1st-order one at  $x = 10^{-4}$  because of the dominance of the 2nd-order quark-quark evolution function at small- $x$  (which comes about because the 1st-order kernel happens to be unusually regular at  $x=0$ ). The gluon distribution in the 2nd order calculation, on the other hand, is lower than that in 1st order at small  $x$  by about 15% at the same  $x$ , due to the fact that the 2-loop evolution kernel is large and negative at small  $x$ . Details of this study can be found in Ref.33

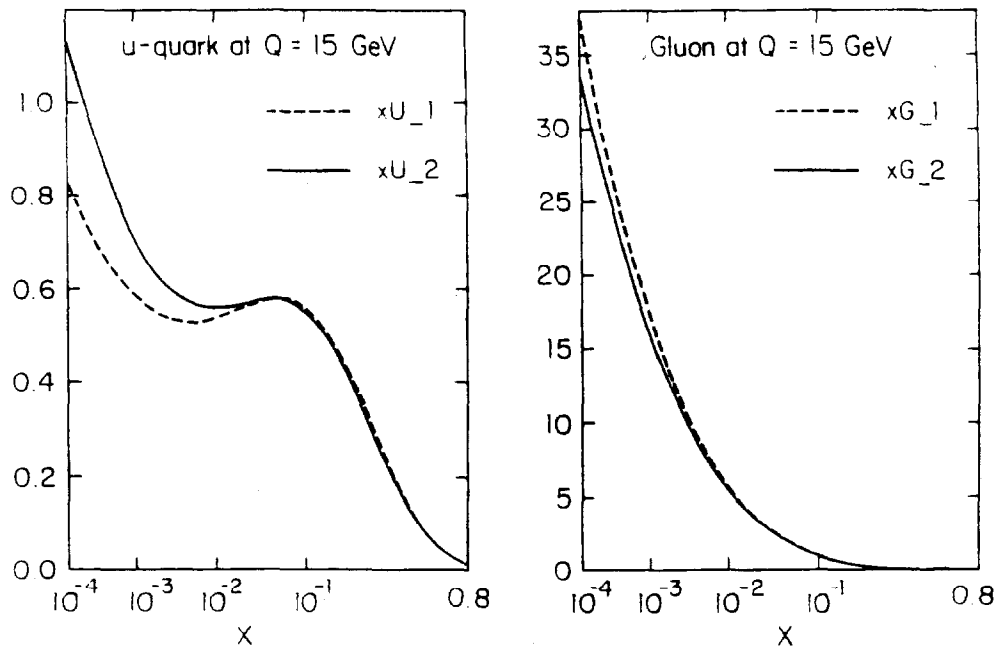


Fig.IV-2: Comparison of 1st and 2nd order evolved u-quark and gluon distributions at  $Q = 15$  GeV.

Most recent parton distribution calculations include 2-loop evolution effects. Ref.33 made direct comparisons with the two widely distributed sets in order to check the consistency of these (relatively complicated) calculations. Agreement was found with one published set (DFLM)<sup>26</sup> but substantial disagreement emerged in comparison to the other (MRS)<sup>27</sup> in the small- $x$  region. Fig.IV-3 shows the comparison, along with the corresponding 1st order results. The latter has since been found to contain a programming error<sup>34</sup> and agreement is obtained after correction of the error. Previous calculations of cross-sections based on these distributions below  $x < 0.01$  must be revised.

For quantitative applications of the QCD parton model incorporating next-to-leading effects, one must also, in principle, take into account the scheme dependence of the parton distributions (cf. Sec.II.C). Ref.33 also compared parton distribution functions in the  $\overline{MS}$  scheme to those in the DIS scheme. The numerical difference is of the order of 10% at  $Q = 4$  GeV. It decreases steadily as  $Q$  increases. Since the Wilson coefficient connecting the

two sets are regular, this effect is not strongly  $x$ -dependent (in contrast to that of the 2nd order evolution kernel).

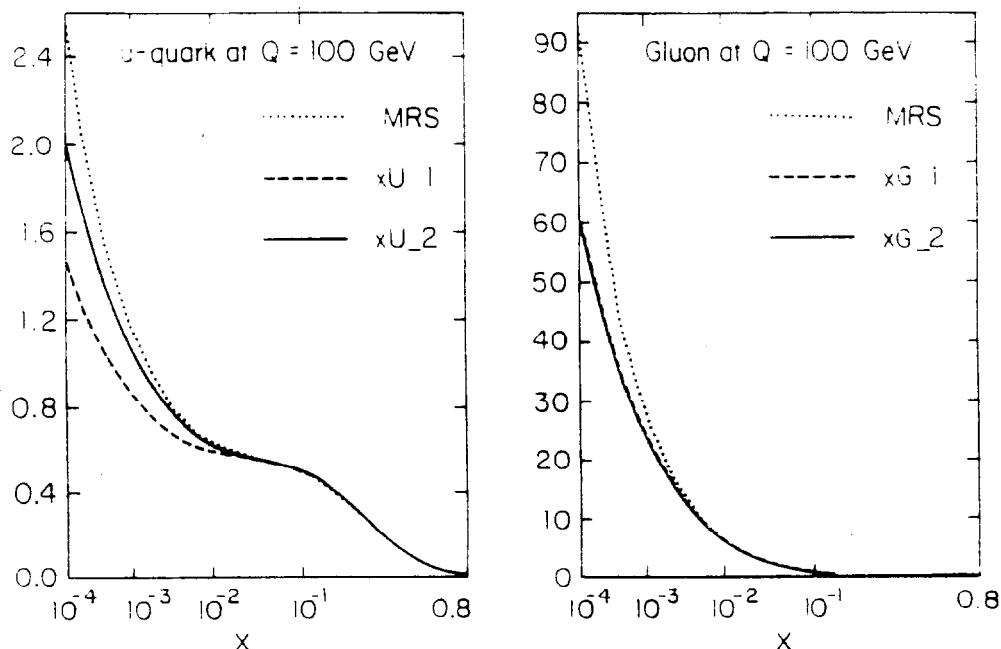


Fig.IV-3: Comparison of 2nd order calculations with MRS distributions.

## V. PROGRAM TO EXTRACT PARTON DISTRIBUTION FUNCTIONS

We have started a program to utilize the data base described above to extract parton distribution functions suitable for quantitative applications of the QCD parton model and for studying the range of possibilities involved in extrapolation to the small- $x$  region beyond directly measured range. For this purpose, we would like to include a wide range of data sets, and to take into consideration as many as possible the relevant experimental factors described in Sec. IV.B. This work is still underway. Here we describe our particular approach and give a progress report on preliminary results.

### A. DESCRIPTION OF METHODS

The first phase of this analysis will be concerned mainly with the latest major experimental data on structure functions measured in high-energy muon- and charged current neutrino-hadron scattering processes for which we have obtained detailed information on -- EMC, CDHSW, and BCDMS. Because of the unresolved discrepancy between some of these experiments, especially in the BCDMS and EMC hydrogen data, it is important to analyze the dependence of the parton distribution parameters on the choice of data. We have systematically evaluated the quality of the fit for various combinations of experimental data sets and compared the parton distributions extracted from these combinations. We will try to answer the question of general concern: Is the well-publicized BCDMS-EMC discrepancy a major hindrance in the determination of a set of good parton distributions? At a later stage, data from other charged current (BEBC, BPF, CCFRR, CHARM, ...) and neutral current experiments (FMM, ...) will be taken into account as well.

In practical applications of the QCD Parton Model, both leading order and next-to-leading order calculations are widely used. Accordingly, our program is set up to perform fits to each of these orders and to compare the results. Discussions given in Sec.IV.C indicate that these fits will result in different extrapolations to the small- $x$  region even if they are fitted to the same data in the currently available energy range. Thus, confronting predictions on hadron collider processes (which typically involve partons with smaller fractional momentum  $x$  than fixed-target ones) based on these distributions may provide good tests of the next-to-leading order QCD Parton Model. Although one expects to be able to fit data with either the 1st or the 2nd order formulas, an interesting question is: whether the 2nd order fits will lead to more stable (hence unique) parton distribution parameters - as they should if the QCD perturbation series indeed makes sense? We shall try to answer this question.

In addition to effects due to experimental systematic errors, heavy-target corrections (the EMC effect), and correlations among measured structure functions, experience shows that the quality and the outcome of a QCD analysis of the parton distributions can also depend on the choice of cuts in  $Q$  and  $W$  in data selection. If the model is applicable in the region where this analysis is made (hence the results are to be trusted), this cutoff dependence must be negligible. Our study includes investigations on this dependence.

One of the most important motivations for undertaking this investigation is to study the range of possibilities of the small- $x$  behavior of parton distributions. Traditional assumptions of the functional form for the initial distributions (at some arbitrarily chosen  $Q_0$ ) over-restrict this behavior. It is important to recognize, for instance, that QCD evolution itself alters the effective functional form assumed for the initial distribution at small- $x$  as soon as the evolution is turned on.<sup>35</sup> Since no particular value of  $Q_0$  is *a priori* special, *it is not natural to assume a specific form for the small- $x$  behavior at a given  $Q$ .* Consequently, *in our study this functional form is left open, to be determined by the fit to data.* We will try to delineate the range of possibilities in the extrapolation of parton distributions to small- $x$ , given all the current data.

An interesting idea about the choice of  $Q_0$  and the associated initial distributions is that of "dynamically generated parton distributions": one assumes that there is some  $Q_0$ , presumably of fairly low value, at which the only effective parton content of the hadron consists of the valence quarks and allow the parton distributions at physically relevant values of  $Q$  be generated solely by QCD evolution.<sup>36</sup> In practice, the value of  $Q_0$  in this scheme has to be so low (certainly below 1 GeV) that the perturbative formalism is not applicable at that scale. Therefore, this parametrization of the initial condition can, at best, be regarded as an effective one chosen for its simplicity. We use this method along with the conventional one for comparison. Our implementation of this approach is somewhat different from the usual one: we include an initial gluon distribution along with the valence quarks; and, instead of arbitrarily fixing  $Q_0$ , we allow its value to be determined by the fit. We can get reasonable fit to data, comparable to other methods, in our preliminary studies. Because this approach starts the evolution at very low  $Q_0$  (our fits typically yield values of about 0.5-0.6 GeV), and because the QCD evolution rapidly accumulates partons at small  $x$ , this approach tends to yield parton distributions at a physical value of  $Q$  which rise more rapidly toward small- $x$  than the conventional approach. (Cf. Ref.36)

With the above considerations in mind, our study is organized in a way best described as a multi-dimensional grid. In the first direction, we have the various factors described above which need to be incorporated in any given fit: (i) heavy target correction (EMC-effect), (ii)



a brief discussion of some preliminary results and tentative conclusions. Details will be described in a forthcoming publication.<sup>38</sup>

**Data Set Selection:** So far the only extensive data sets for which we have detailed information on are: EMC (iron, hydrogen & deuterium), CDHSW (iron) and BCDMS (hydrogen & carbon). We have carried out fits to these data sets individually and in various combinations in order to check the discriminating power of the data sets, the consistency between them, and to determine the stability of the extracted parton distributions and the QCD coupling scale parameter ( $\Lambda_{\text{QCD}}$ ) against the choice of data sets. We obtain very good fits to the combined CDHSW & EMC and for the combined CDHSW & BCDMS data sets, typically  $\chi^2$  per dof of 1 or less (for details, see dependence on  $Q^2$ -cut below); and we also obtain reasonable fits to the combined data sets of all three experiments with slightly higher  $\chi^2$  (1.0 to 1.3 per dof depending on  $Q^2$ -cut). Fig.V-2 gives a global view of the quality of a typical fit to the full combined set. The format of this rather busy figure follows that of Fig.IV-1 in Sec.IV. We shall come back to discuss the some features of this fit after examining the  $Q^2$ -cut dependence.

**Systematic Errors:** For most of our fits, the systematic error is added in quadrature to the statistical error point-by-point. Correlation of errors have not yet been taken into account, as explained earlier. Separate fits have been done with systematic errors ignored (as done by most previous studies) in order to assess their effect on the results. We found the quality of fit depends critically on whether the experimental systematic errors are included, in particular when multi-sets of data from different experiments are used. The  $\chi^2$  per degree of freedom typically jumps from around 1 to 3 - 5 (depending on the  $Q^2$ -cut used) when systematic errors are left out. Also, the shapes of the extracted distributions are modified, and the value of QCD-lambda becomes rather unstable against changes in other variables such as  $Q^2$ -cut.

**Heavy Target (EMC-effect) Corrections:** Since the objective is to extract parton distributions inside the *proton*, we apply a heavy target correction to the iron and carbon data before combining these in a fit with hydrogen and deuterium data. The x-dependent correction factor is taken from an empirical formula derived from the measured ratio of  $F_2(\text{iron})/F_2(\text{deuterium})$  (EMC) and  $F_2(\text{carbon})/F_2(\text{deuterium})$  (BCDMS). No Q-dependence of this factor is included as there is no clear experimental evidence for it. Leaving out this correction (as some existing parton distribution analyses have done) typically does not affect the quality of the fit (as measured by the chi-square per dof) by much. However, the shapes of the extracted parton distributions are clearly changed.

**1st vs. 2nd Order QCD Evolution:** We have tried to extract parton distributions from the same set of data using both the 1st order and the 2nd order QCD parton model formulas (cf. Sec.II.B,C. We find satisfactory fits in each case. This is expected, as the discussion in Sec.IV.C indicated that the 2nd-order evolution differs little from the 1st order one for  $x > 0.01$ , provided the value of QCD- $\Lambda$  is appropriately adjusted. The shape parameters of the parton distributions extracted from these analyses are close to each other, as they should be. The parameters obtained with the 2nd order fits are somewhat more stable against changes in other variable (cf. the paragraph on  $Q^2$ -cut below).

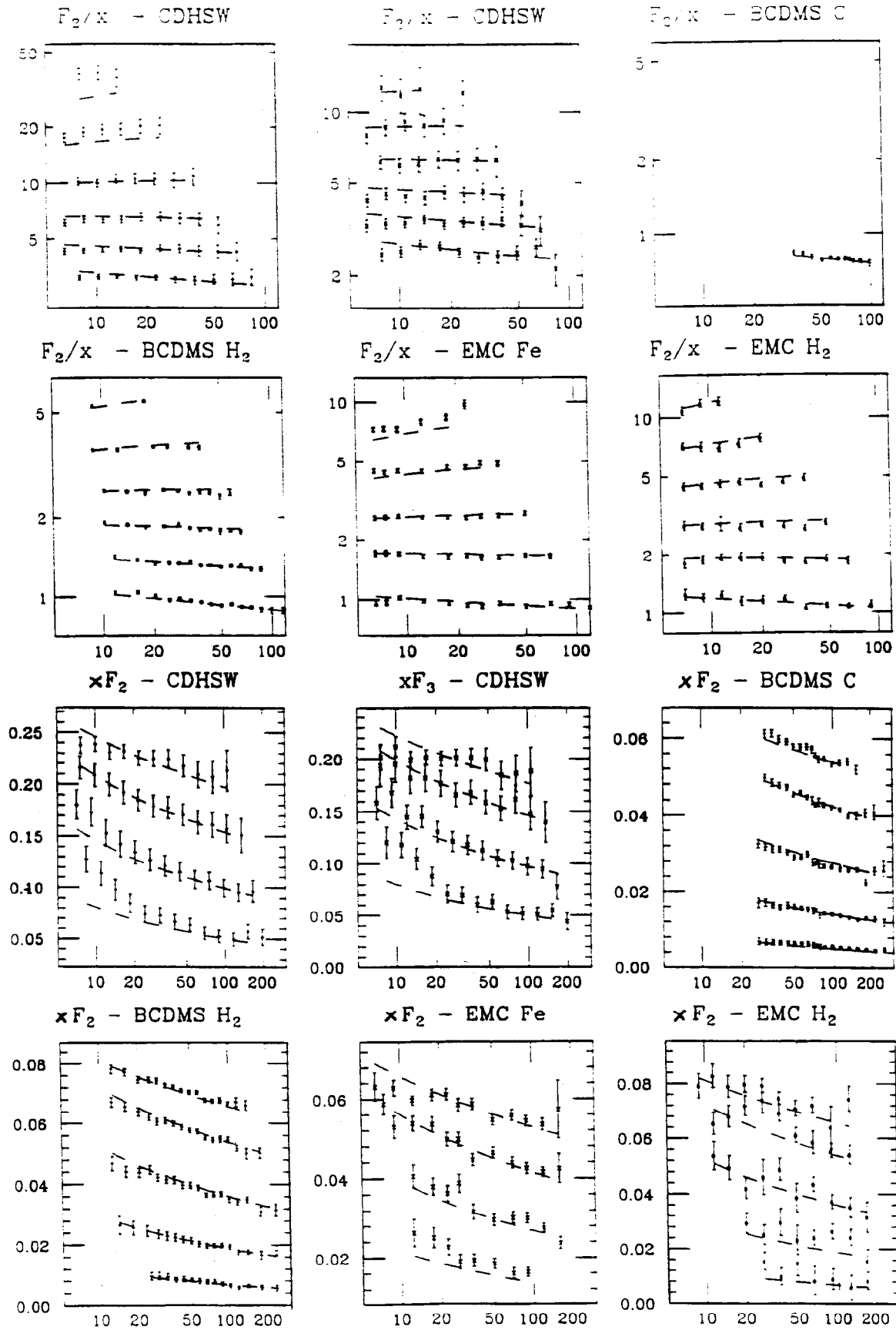


Fig.V-2: Sample fit to combined data sets of CDHSW ( $F^2$  &  $F^3$ ), BCDMS (C & H<sub>2</sub>), and EMC (Fe & H<sub>2</sub>). The  $Q^2$ -cut used is 6.25 GeV<sup>2</sup>. The Dashed lines represent the fit. The top six plots are for  $x < 0.3$ . The bottom six plots are for  $x > 0.3$ . The specific values of  $x$  for the data points are the same as those shown in Fig.IV-1.

**Q<sup>2</sup>-cut Dependence:** If we are in the kinematic region where perturbative (twist-2) QCD is a good approximation, the results of our fits should not depend on the choice of Q<sup>2</sup>-cut in our selection of data. In practice, the question of Q<sup>2</sup>-cut is important for at least two reasons: (i) twist-4 as well as non-perturbative effects come in at low values of Q<sup>2</sup>. We do not know a priori when do these effects set in; (ii) the discrepancies between existing data sets, especially that between EMC and BCDMS are x- and Q-dependent. For fits to the three different combinations of data sets described in a previous paragraph and for calculations performed with both 1st and 2nd order QCD formulas, we have systematically varied the Q<sup>2</sup>-cut in the range 6.0 to 25 GeV<sup>2</sup> to observe its effect.

The stability of the shape parameters and  $\Lambda_{\text{QCD}}$  against the Q<sup>2</sup>-cut can depend on the choice of the parametrization scheme. The following summary only applies to the relatively economical parametrization scheme described earlier in this section. We found the value of  $\Lambda_{\text{QCD}}$  to be relatively stable against variations of Q<sup>2</sup>-cut in a series of fits for a given choice of data set and calculational scheme. Some typical results are presented in Fig.V-3

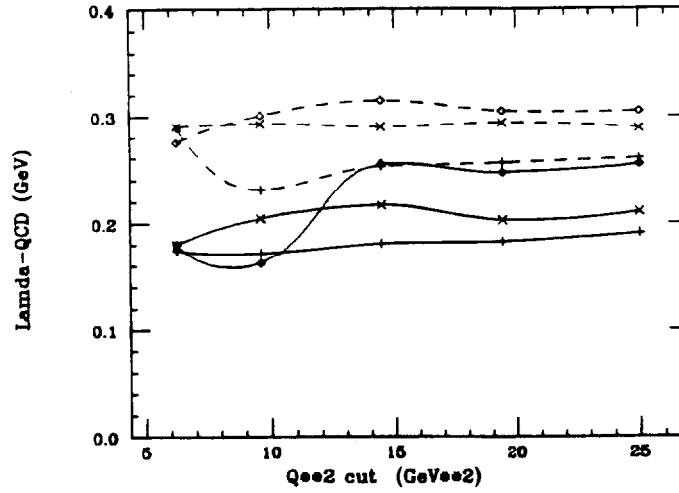


Fig.V-3: Value of  $\Lambda_{\text{QCD}}$  vs. Q<sup>2</sup>-cut obtained in various fits. Points connected by the top three curves are from 1st order fits to BCE, CE, and BC data sets in descending order; those connected by the bottom three curves are from the corresponding 2nd order fits. (Here BC = BCDMS + CDHSW; CE = CDHSW + EMC; and BCE = all three.)

Since the meaning of  $\Lambda$  is ambiguous, depending on the number of active flavors and on the order of perturbation used, we have converted all  $\Lambda$  values to their 1st order 4-flavor equivalent (so that the QCD couplings are the same) for this comparison. For the 2nd order fits, the true 2nd order 4-flavor  $\Lambda$  value,  $\Lambda(2,4)$ , is related to the equivalent 1st order value,  $\Lambda(1,4)$ , given above by a very accurate formula  $\text{Log}_{10}\Lambda(2,4) = 0.156 + 0.81 \cdot \text{Log}_{10}\Lambda(1,4)$ . We will comment more on these results in the discussion section.

The parameters which characterize the initial parton distributions at a given Q<sup>2</sup> (say Q<sub>0</sub><sup>2</sup>=10 GeV<sup>2</sup>) are also found to be generally stable against variations in Q<sup>2</sup>-cut, although some more so than others. A detailed description will necessitate a full discussion of our parametrization formulas which space does not allow here. We give as an example the most Q<sup>2</sup>-cut-dependent parameter we found which is the exponent B to the (1-x) factor in the gluon distribution. We see that this parameter depends rather sensitively on the choice of data set. This is one of the manifestations of the well-known fact that the shape of the

gluon distribution is closely coupled to the value of  $\Lambda_{\text{QCD}}$  which, as shown above, also differs in the various fits. Within a given data set, the value obtained for  $B_G$  is rather stable, especially for 2nd-order fits and for  $Q^2$ -cut above 15  $\text{GeV}^2$ .

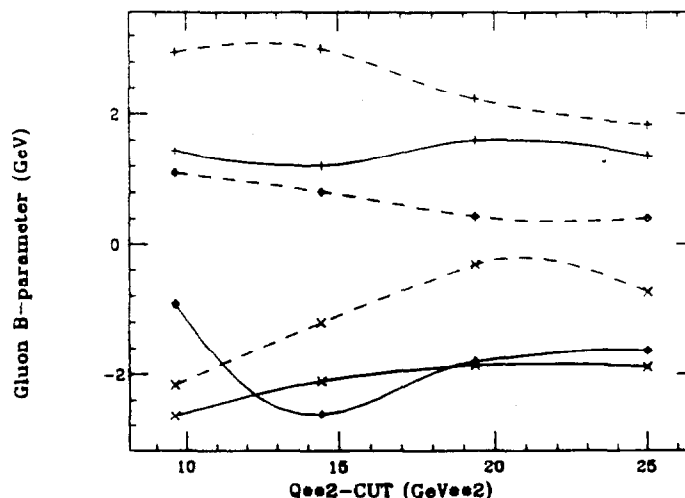


Fig.V-4: Gluon B-parameter vs.  $Q^2$ -cut from various fits. The B-parameter is normalized to 0 with respect to the MRS-E distributions at  $Q^2=10 \text{ GeV}^2$ . The labelling of the points is the same as in Fig.V-3.

### C. TENTATIVE OBSERVATIONS AND CONCLUSIONS

*Do disagreements between existing experiments preclude a meaningful parton distribution analysis?*

The answer is not an obvious yes. A meaningful QCD parton model analysis must invoke a reasonable  $Q^2$ -cut in the selection of data to minimize higher-twist and non-perturbative effects. With increasing  $Q^2$ -cut, the well-publicized disagreements between BCDMS and EMC experiments become less significant. Therefore, we have been able to obtain reasonable QCD fits to the combined BCDMS-CDHSW-EMC data above  $Q^2$  10-15  $\text{GeV}^2$ . Perhaps somewhat unexpectedly, in a typical fit, points which contribute the most to the  $\chi^2$  turn out to come from the two lowest  $x$  bins and the highest  $x$  bin of the new CDHSW experiment and the EMC-Fe experiment rather than from the BCDMS and EMC hydrogen data points, as illustrated in Fig.V-2. This is due to the statistical weight of the hydrogen data (with very small errors), and due to the fact that an overall normalization factor for each experiment is allowed as a fitting parameter. We found that these fits favor a normalization factor of  $\approx 0.95$  for the BCDMS data points, and a factor of  $\approx 1.03$  for the EMC points, both with respect to those of CDHSW.

We do get better fits with combined data from only two out of these three experiments - BCDMS-CDHSW or CDHSW-EMC -- as compared to the all-inclusive fits discussed above ( $\chi^2$  per dof 0.7-1.0 compared to 1.0-1.3). And the fitting parameters from these fits also seem to be a little more stable than from the grand combined fits, as one may see in Figs.V-3 and V-4. However, the difference does not seem to be very significant. We emphasize that it is possible to reach this conclusion only if the systematic errors of the experiments are fully taken into account and if a healthy  $Q^2$ -cut is imposed. To illustrate this point, a sample fit with  $Q^2$ -cut = 20  $\text{GeV}^2$  is shown in Fig.V-5. The quality of this fit is clearly better than

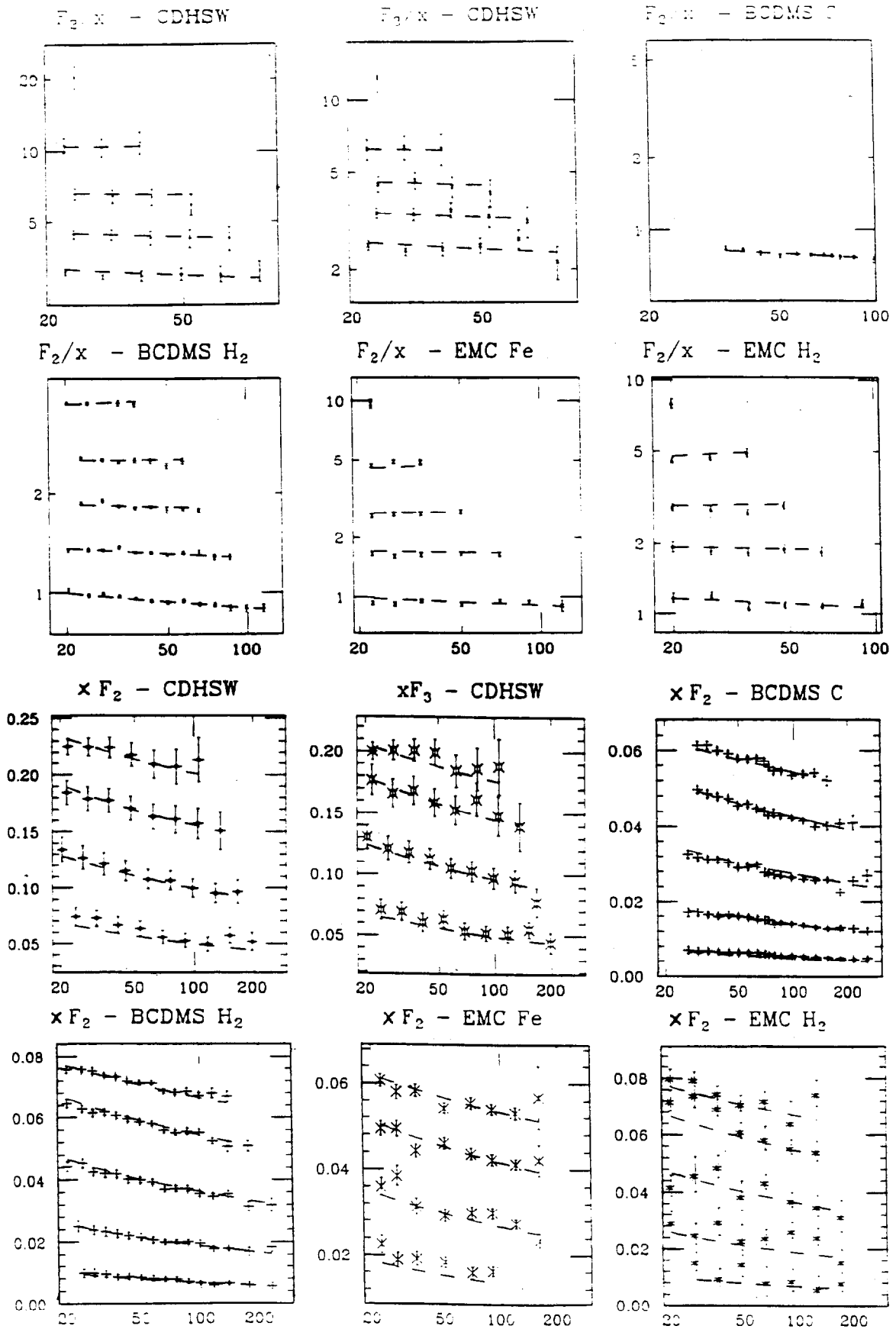


Fig.V-2: Sample fit to combined data sets of CDHSW ( $F^2$  &  $F^3$ ), BCDMS (C & H<sub>2</sub>), and EMC (Fe & H<sub>2</sub>). The  $Q^2$ -cut used is 20 GeV<sup>2</sup>. The Dashed lines represent the fit. The top six plots are for  $x < 0.3$ . The bottom six plots are for  $x > 0.3$ . The specific values of  $x$  for the data points are the same as those shown in Fig.IV-1.

that shown in Fig.V-2. The improvement almost exclusively come the exclusion of the low Q points.

*What do existing data tell us about the small-x behavior of parton distributions?*

The answer is: not very much. The lowest values of x included in our analyses are in the range 0.03 - 0.05, depending on  $Q^2$ -cut. The small-x extrapolation of the fitted parton distributions is mainly controlled by the parameter A which is the exponent in the standard factor  $x^A$  in the distribution function (at the initial  $Q^2$ , usually chosen to be  $10 \text{ GeV}^2$  in our calculations). The values of A for (x times) the gluon and the sea-quark distributions we obtain are very stable within a given set of fits, but differ from set to set. The results are summarized in the following table.

	BCDMS CDHSW	CDHSW EMC	All Combined
1st Order	0.303	-0.05	0.305
2nd Order	0.340	-0.01	0.085

Table V-1: Exponent parameter A obtained in various fits (normalized to 0 with respect to the MRS-E distributions at  $Q^2 = 10 \text{ GeV}^2$ ).

The different values will give rise to very different small-x extrapolations to small-x values below  $10^{-3}$ . However, we can also get acceptable fits to each set of data by fixing this parameter at any value close to the range above. For instance, if the BCDMS-CDHSW set is fit with fixed  $A = -0.2$ , the  $\chi^2$  per dof only increases from 1.06 to 1.17. Of course, when this is done, some of the other parameters (e.g.  $\Lambda_{\text{QCD}}$ ) also change from their best-fit values.

*How well can one determine  $\Lambda_{\text{QCD}}$  and the initial parton distributions from the DIS data?*

We confirm the known answer: the u- and d-quark distributions are fairly well determined, but the other parameters are correlated and not so well constrained. We have seen from Figs.V-3 and V-4 and the last paragraph that the extracted values of  $\Lambda_{\text{QCD}}$  and parton shape parameters do vary from one set of fits to another. In this regard, the "stability" of the fitted values for some parameter within a given set of fits can be misleading. The range of variation spanned by the various sets of fits is a better indication of the uncertainties involved. A reliable way to determine the uniqueness of the extracted parameters is to perform a full error analysis in the fitting process (e.g. by invoking MINOS inside MINUIT). We found that MINUIT will not yield meaningful error quotes on  $\Lambda_{\text{QCD}}$  and the gluon distribution parameters unless most other parameters are artificially fixed.

To conclude: many uncertainties on the parton distributions in QCD fits to current deep inelastic scattering data are intrinsic to the problem because the number of combinations of these distributions measured by the structure functions are limited. This is especially true for the gluon since it does not couple directly to the electroweak currents, and also for the anti-quarks since they contribute only a small part to the measured cross-section. These uncertainties can make a fitting program ambiguous. The only way to remedy this problem is to supplement deep inelastic scattering with complementary processes which involve gluons and anti-quarks in a direct way. Well-known examples are Drell-Yan processes (W-, Z-production, as well as continuum lepton pairs), direct-photon production, heavy-flavor

production. ... etc. Any serious study of the parton distributions must take these processes into account. We certainly plan to incorporate these processes in our analysis at a later stage.

## VI. ROLE OF CURRENT AND FUTURE EXPERIMENTS IN THE DETERMINATION OF PARTON DISTRIBUTIONS

In the continuing effort to determine the parton distributions in the QCD Parton Model beyond the currently available energy range, we must have more and better experimental data in a variety of processes. As illustrated on the map of kinematic variables, Fig.I.2, we must use available hadron collider processes (at the  $S\bar{p}pS$  and the Tevatron) to extend the coverage to smaller  $x$ , in addition to supply information on the gluon and anti-quarks. Eventually, HERA will expand the kinematic range by two orders of magnitude when it becomes operative. This section summarizes the opportunities offered by the various forthcoming experiments and facilities.

### A. FIXED TARGET LEPTON-HADRON SCATTERING

Although extensive data on deep inelastic scattering structure functions from fixed-target experiments already exist, the glaring discrepancy between major high-statistics experiments, especially for hydrogen target, cries for a resolution by further accurate experiments. In the years ahead, we can look forward to:

- \* The CCFR Collaboration at Fermilab have a sample of 250,000 anti-neutrino and 1,500,000 neutrino events for energies in the range 0-600 GeV from their 1985 and 1987 runs. Structure functions are expected in early 1989.
- \* The NMC collaboration (an upgraded version of EMC) currently underway at CERN;
- \* The Fermilab Muon collaboration (Expt. E665). This Tevatron Muon collaboration at FNAL have several million deep inelastic scattering events recorded during their 1987 run at 500 GeV. Their data extend to  $x$  of 0.001. However, the experiment is not designed to optimize the measurement of structure functions.

In addition, some entirely new experiments are being considered at Fermilab and UNK.

### B. HERA

HERA, projected to come into operation in 1990, will extend measurement of the structure functions to about 0.0001 in  $x$  and about 1,000  $\text{GeV}^2$  in  $Q^2$ , as shown in Fig.I-2. Since the event rate is very high for small  $x$ , the structure functions can be measured with good accuracy in this important region. In view of the lack of reliable experimental data below  $x \approx 0.05$ , and the importance of this information for the study of physics in future colliders, the importance of the HERA measurements cannot be over-emphasized. The capabilities of HERA have been extensively documented in various HERA study reports.<sup>39</sup> For the purpose of this review, we shall only highlight its unique potential to measure the gluon distribution.

The definitive method for determining the gluon distribution is to measure the longitudinal structure function (the difference between  $F^2$  and  $F^L$ , Eq.(II-6)). The basic

formula in the QCD parton model which defines the gluon distribution inside the hadron in terms of  $F^{Long}$  is given by Eqs.(II-26). (Cf. also Figs.II-1b and II-2c.) This method requires the measurement of the cross-section at several collision energies.  $F^{Long}(x,Q)$  is determined from the slope of a straight-line plot of the cross-section versus a suitably chosen variable (commonly called  $\epsilon$ ) for fixed  $(x,Q)$  -- the classic "Rosenbluth Plot".<sup>40</sup>

In order to gain some feeling on what can be achieved, we give a brief description of some relevant experimental details. For definiteness, we consider here a specific detector, namely ZEUS.<sup>41</sup> The overall kinematically accessible  $x$  and  $Q^2$  range is shown in Figure VI-1, bounded by the curve labelled "before cut". Several cuts must be applied to simulate detector acceptance:

- o a 200 mrad cut is applied on the angle of the scattered electron with respect to the beam to ensure that it will enter the rear detector.
- o the electron is required to have a transverse momentum of at least  $3\text{GeV}/c$  for it to be well separated from the fragmentation jet;
- o a cut of  $y < 0.83$  is applied to stay away from regions where radiative corrections are changing rapidly.<sup>42</sup>

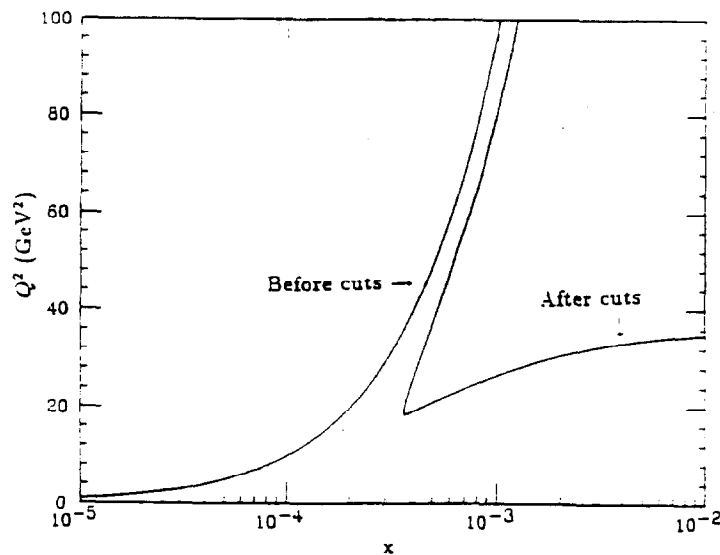


Fig.VI-1: Available low  $x$  and  $Q$  range in the ZEUS detector.

The resultant  $x$  and  $Q^2$  range available after the cuts is bounded by the curve labelled "after cut" in Fig.VI-1. The  $P_T$  cut places the largest restriction on  $x$  while the angle cut has the largest effect on the minimum  $Q^2$ .

Fig.VI-2 shows the anticipated ability to resolve between two representative gluon distributions<sup>40</sup> at  $Q^2 = 50 \text{ GeV}^2$  for initial gluon distributions of the form: A)  $xG(x, Q^2) = 0.676x^{-1/2}(1-x)^5$  and B)  $xG(x, Q^2) = 5(1-x)^9$ . The error bars indicate the size of the statistical error expected for  $100\text{pb}^{-1}$  of luminosity, and the shaded band shows the expected size of systematic errors, which include a 5% luminosity error and systematic errors on  $N$  (the number of events in an  $x, Q^2$  bin) and  $\Gamma$  due to resolution effects. Note that the relative luminosity errors for different  $\epsilon$  can be removed by using high  $x$  data. According to this study, these distributions will be easily distinguishable.

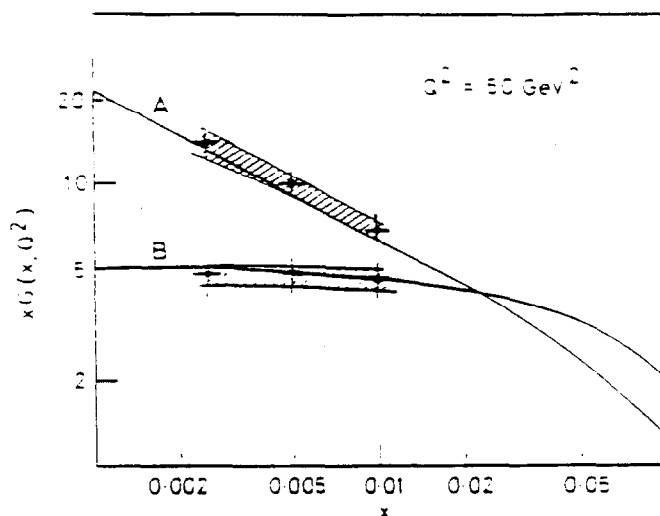


Fig.VI-2: The anticipated resolving power on the small- $x$  behavior of the gluon distribution at HERA.

An alternative method to measure the gluon distribution at HERA has been proposed.<sup>43</sup> This utilizes the cross-section for  $J/\psi$  production and assumes that it is dominated by the photon-gluon fusion mechanism.<sup>44</sup> Details can be found in ref.43. Whereas this certainly provides an interesting window to test the gluon distribution, it cannot provide a true measurement for the latter because of the uncertain theoretical basis for the underlying interaction mechanism. There is no unambiguous order-by-order perturbative QCD formula for this process.

With results now available from the detailed parton distribution analyses described in Sec.V, we plan to investigate the resolving power of the HERA experiments concerning the major remaining uncertainties on the parton distributions: the shape of the gluon distribution and on the extrapolation to small- $x$ .

### C. DRELL-YAN PROCESS

Next to deep inelastic scattering, the production of lepton-pairs (via a virtual  $\gamma$ ), and  $W$ - and  $Z$ -production by the Drell-Yan mechanism (and its higher order generalizations) are the cleanest in terms of its QCD parton model foundation. The basic processes involved are shown in Fig.VI-3. It is very important to measure the cross-section for these processes at the current and future colliders for two major reasons: (i) as is apparent from Fig.VI-3, these processes receive substantial contribution from the gluon through the quark-gluon "Compton scattering" mechanism, hence provide a much needed handle on the gluon distribution; and (ii) the continuum lepton-pairs probe an  $x$ -range much lower than that given by fixed target DIS experiments, hence furnish us with valuable information on the trend of small- $x$  extrapolation of the parton distributions. Specifically, since  $x_1 x_2 = Q^2/s$ , one can reach below  $x = 10^{-3}$  at the Tevatron for lepton-pairs produced away from the central region. This is to be compared to  $x > 0.05$  in existing deep inelastic scattering.

Drell-Yan cross-section from fixed-target experiments have been used in the extraction of parton distributions in some of the sets reviewed in Sec.IV. The sensitivity of the projected cross-section, both total and differential, to different assumptions about the small- $x$  behavior of the parton distributions have been systematically studied during the 1987 Madison Workshop<sup>45</sup> in the context of a general survey of all promising "small- $x$  processes".

It was found, by a leading order Monte Carlo study, that in addition to the obvious dependence of the total cross-section on the assumed parton luminosity at small- $x$ , the shape of the differential  $y$ -distribution of the Drell-Yan process is extremely sensitive to the small- $x$  behavior of the parton distributions.

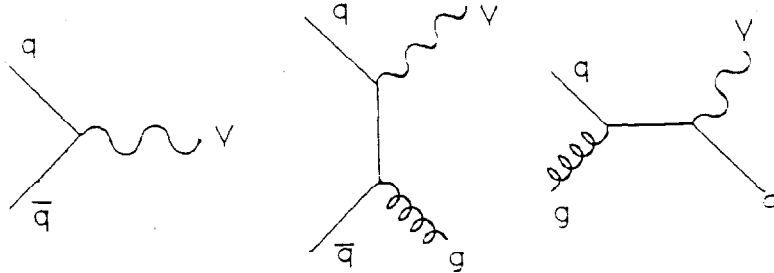


Fig.VI-3: Leading and Next-to-leading Drell-Yan processes.

In view of recent awareness of the importance of higher order calculations, in particular for small- $x$ , we have carried out a next-to-leading order calculation of the Drell-Yan cross-section during this Workshop.<sup>46</sup> The results confirm the conclusions of the previous study. In Fig.VI-4a we show the next-to-leading order results on this  $y$ -distribution at the Tevatron energy obtained by using parton distributions with assumed  $x^{-1}$  behavior (solid curve) and with assumed  $x^{-1.5}$  behavior (dashed curve) at  $Q = 3.0$  GeV and evolve with 2-loop evolution kernel to  $Q = 15.0$  GeV. In Fig.VI-4b, we show the corresponding results at the SSC energy. We see that the shape of these curves provide a good handle on the assumed small- $x$  behavior. Even without measuring the full  $y$ -range, the ratio between the cross-sections at the central region and some forward region can already yield valuable information on the behavior of parton distributions at small- $x$ . More detailed study of the discriminating power of this type of measurement starting from the results of Sec.V is clearly worthwhile.

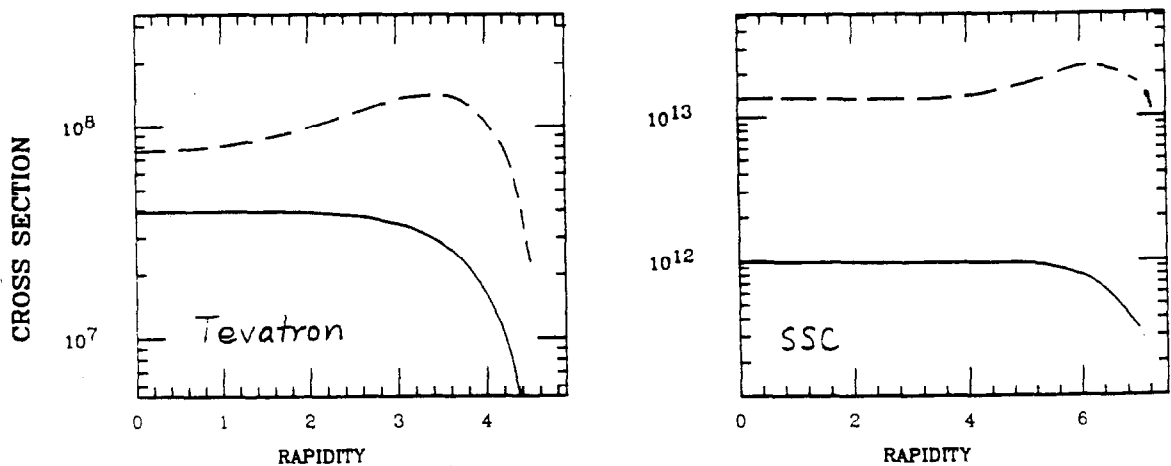


Fig.VI-4: Next-to-leading order  $y$ -distr. of Drell-Yan Cross-section for two assumed small- $x$  extrapolations: (a) Tevatron I; (b) SSC

## D. DIRECT-PHOTON PRODUCTION

Details on direct photon production is covered in another contribution to these proceedings.<sup>47</sup> It is worthwhile mentioning, however, that this process can have an important role in the overall scheme of determining the parton distributions. The basic underlying mechanism is very similar to the case of Drell-Yan processes discussed above. It is sensitive to the gluon distribution. And 2nd order QCD formulas for the cross-section do exist.

## VII. SUMMARY

In this report we reviewed the current status of deep inelastic scattering structure functions and parton distributions in the QCD parton model. We spelled out explicitly the necessary theoretical framework for QCD analyses in the leading and the next-to-leading order. Likewise, we discussed important experimental analysis issues in the measurement of structure functions and in the subsequent process of extracting parton distribution functions.

In order to make maximum use of recent experiments with vastly increased statistics, it is important to have a data base with complete information on all existing data in easily accessible form and in a common format. We have been working to assemble such a complete database. An important part of this effort consists of incorporating detailed information on systematic errors and analysis assumptions which will allow better estimates of the errors on physical quantities extracted from these data.

We also presented a review of widely used parton distributions and showed the need for a more up-to-date analysis using current data and incorporating significant experimental and theoretical considerations relevant for contemporary applications of the QCD parton model, particularly attention to the small- $x$  behavior and next-to-leading order effects. We reported on our own program to carry out such an analysis and presented preliminary results and conclusions from this extensive work.

We underlined the important roles that current collider processes and upcoming HERA measurements can play in complementing the structure function analysis for the complete determination of the parton distributions. We highlighted the Drell-Yan process and direct photon production at the colliders as the most crucial in providing information on the gluon distribution in general and all parton distributions in the small- $x$  region in particular. This will be important for its own sake as well as for providing a vital constraint in the extrapolation to even smaller  $x$  needed for the study of most SSC physics processes.

## ACKNOWLEDGEMENT

We would like to thank our colleagues at the Snowmass Workshop, especially members of the QCD group, to which this subgroup belonged, for stimulating discussions. WKT would also like to thank John Collins for useful discussions and suggestions.

#### REFERENCES

- <sup>1</sup> For a recent review, see K. Ellis. Review talk given at the 1988 Munich Conference on High Energy Physics. Fermilab Preprint, 1988.
- <sup>2</sup> For comprehensive reviews and complete lists of references, see G. Altarelli, Phys. Rep. 81C, 1 (1982); W. Furmanski and R. Petronzio, Z. Phys. C11, 293 (1982).
- <sup>3</sup> EMC Fe: Aubert et al., Nucl. Phys. B159, 189 (1985).
- <sup>4</sup> BCDMS C: Benvenuti et al., Phys. Lett. B195, 91 (1987)
- <sup>5</sup> BFP Fe: P. Meyers et al., Phys. Rev D34, 1265 (1986).
- <sup>6</sup> CCFRR Fe: MacFarlane et al., Z. Phys. C26, 1-12 (1984); MacFarlane, Nevis preprint 1297 (1984), Purohit, Nevis preprint 1298 (1984).
- <sup>7</sup> CDHS: Abramowicz et al., Z. Phys. C17, 283 (1984); Z. Phys. C25, 29 (1984); Z. Phys. C35, 443 (1984); CDHSW: B. Vallage, DPhPE (Saclay) CEA-N-2513 (in French)
- <sup>8</sup> FMM: P. Mattison et al. Phys. Rev. Lett. 55, 574 (1985); and MIT Ph.D. Thesis (1987)
- <sup>9</sup> BCDMS H: Benvenuti et. al. Preprint JINR-E1-87-689.
- <sup>10</sup> EMC H: Aubert et al., Nuclear Phys. B259, 189 (1985).
- <sup>11</sup> R. Mount, talk given at 1988 Munich International Conference on High Energy Physics.
- <sup>12</sup> "EMC-effect": Aubert et al., Nucl. Phys. B272, 158 (1986)
- <sup>13</sup> SLAC E140: S. Dasu, et al., Phys. Rev. Lett. 60, 2591 (1988).
- <sup>14</sup> EMC': J. Ashford et al., Phys. Lett. 202B, 603 (1988).
- <sup>15</sup> K. Lassila et. al., Phys. Lett. 209B, 343 (1988).
- <sup>16</sup> E. Berger & J. Qiu, Preprint ANL-HEP-88-42 (1988).
- <sup>17</sup> F. E. Taylor, Proc. 13th Int. Conf. on Neutrino Physics and Astrophysics, Medford, MA (1988).
- <sup>18</sup> S. Dasu, et. al., Phys. Rev. Lett. 61, 1061 (1988)
- <sup>19</sup> R. Voss, in Proc. of 1987 International Symposium on Lepton and Photon Interactions at High Energies, Hamburg, 1987.
- <sup>20</sup> I.A. Savin, (private communication)
- <sup>21</sup> Benvenuti et al., Phys. Lett. 195B, 97 (1987); and JINR preprint JINR-E1-87-699 (1987).
- <sup>22</sup> BEBC: D. Allasia et al., Z. Phys. C28, 321 (1985); Phys. Lett. 135B, 231 (1986); Varvell et al. CERN/EP 87-46 (1987).

- <sup>23</sup> R.N. Barnett, Phys. Rev. Lett. 36, 1163 (1976); B.J. Edwards, T.D. Gottschalk, Nucl. Phys. **B186**, 309 (1981); B.J. Kaplan, F. Martin, Nucl. Phys. **B115**, 333 (1976); C.H. Lai, Phys. Rev. **D18**, 1422 (1978); H. Georgi, H.D. Politzer, Phys. Rev. **D14**, 1829 (1976)
- <sup>24</sup> CHARM: Bergsma et al., Phys. Lett. **123B**, 269 (1983); *ibid.* **153B**, 111 (1985); Allaby et al., Phys. Lett. **B197**, 281 (1987).
- <sup>25</sup> Gluck et al, Z. Phys. **C13**, 119 (1982)
- <sup>26</sup> D. Duke and J. Owens, Phys. Rev. **D30**, 49(1984).
- <sup>27</sup> E. Eichten et. al., Rev. Mod. Phys. **56**, 579 (1984), and Erratum **58**, 1065 (1986)
- <sup>28</sup> M.Diemoz, F.Ferroni, E.Longo & G.Martinelli, Z. Phys. **C39**, 21 (1988)
- <sup>29</sup> A.D.Martin, R.G.Roberts & W.J.Stirling, Phys. Rev. **D37**, 1161 (1988).
- <sup>30</sup> B. Vallage, Thesis submitted to Universite de Paris Sud.
- <sup>31</sup> P. Berge et al., Z. Phys. **C35**, 443 (1987); Allaby et al., Z. Phys. **C38**, 403 (1988).
- <sup>32</sup> Proceedings of the 1984 Summer Study on the Design and Utilization of the SSC, Ed. R. Donaldson and J. Morfin, (1985); and Proceedings of the 1986 Summer Study on the Physics of the SSC, Ed. R. Donaldson and J. Marx, (1987).
- <sup>33</sup> Wu-Ki Tung, "Small-x Behavior of Parton Distribution Functions in the Next-to-leading Order QCD Parton Model", Nucl. Phys. (To be published), Fermilab-PUB/88-135-T.
- <sup>34</sup> R. Roberts, private communication.
- <sup>35</sup> J.C. Collins, S. Lomach, and F. Olness, IIT preprint (1988).
- <sup>36</sup> M. Gluck, R.M. Godbole, & E. Reya, (Dortmund U.), DO-TH-88/9 and DO-TH-88/18 (1988).
- <sup>37</sup> Wu-Ki Tung (to be published).
- <sup>38</sup> J.G. Morfin and Wu-Ki Tung (to be published).
- <sup>39</sup> See for example, R. Brinkman "HERA" DESY-HERA-88-03 (1988).
- <sup>40</sup> For details, see Cooper-Sarkar et al., Z. Phys. **C39**, no. 2, 1988.
- <sup>41</sup> ZEUS Collaboration, Technical Proposal (March 1986); ZEUS Collaboration, Status Report (September 1987).
- <sup>42</sup> C. Kiesling, Proc. DESY Theory Workshop, 1987.
- <sup>43</sup> S.M. Tkaczyk, W.J. Stirling, D.H. Saxon, RAL-88-041. G.A. Schuler, DESY Preprint, DESY 87-114.

- <sup>44</sup> E.L. Berger, D. Jones, Phys. Rev. D23 (1981) 1521; and A.D. Martin, C.K. Ng and W.J. Stirling; Phys. Letters B191 (1987) 200.
- <sup>45</sup> F. Olness and W.K. Tung, Int. Journal of Mod. Phys. A2, 1413 (1987); also in Proceedings of International Conference on From Colliders to Super-colliders, Madison, World Scientific (1987).
- <sup>46</sup> J.C. Collins, F. Olness, and Wu-Ki Tung, (to be published).
- <sup>47</sup> I. Hinchliffe and M. Shapiro, these proceedings.